Effects of wave load models on the uplift risk of ports exposed to hurricanes.

Effects of wave load models on the uplift risk of ports exposed to hurricanes.

By

GEORGIOS E. EFSTATHOPOULOS, B.A.Sc., M.ENG

A Thesis Submitted to the School of Graduate Studies in Partial Fulfillment of the Requirements for the Degree Master of Applied Science

McMaster University

MASTER OF APPLIED SCIENCE (2022) (Civil Engineering)

McMaster University Hamilton, Ontario

TITLE:	Effects of wave load models on the uplift risk of ports exposed to hurricanes.
AUTHOR:	Georgios E. Efstathopoulos, B.A.Sc., M.ENG.
SUPERVISOR:	Dr. Georgios Balomenos
NUMBER OF PAGES:	ix - 80

ABSTRACT

Pile-supported ports allow seawater to run below the deck, and thus may suffer structural damages during extreme coastal events such as hurricanes. These structural damages, in turn, may result to port closures that can cause significant economic losses. Risk analysis can predict the post-hazard functionality of ports though the structural damage assessment of these structures prior to coastal events. However, assumptions on the selected demand estimates may affect the estimated probability of structural damage.

This research aims to shed light on the sensitivity of the wave model selection for the risk assessment of pile-supported ports when subjected to storm surge and waves. The examined structural damage is the uplift of the deck, and the risk assessment is conducted through the development of fragility curves for a typical deck-pile connection, for which fragility curves are developed for different wave models. Uncertainties are also considered in parameters affecting the demand and capacity of the examined deck-pile connection and are propagated through the Monte Carlo simulation using the Latin Hypercube Sampling. The results indicate changes to the uplift probability as a result of the selected wave model. Thus, wave model selection can alter the uplift failure probability. In addition, the study proposes parameterized fragility models to enable the uplift risk assessment across a region. The presented results aim to throw light on the proper model selection to produce more realistic risk assessment estimates towards the resilience of coastal infrastructure.

ACKNOWLEDGEMENTS

First of all, I would like to express my gratitude to my supervisor Dr. Balomenos for his support, encouragement, and academic guidance. It has been my privilege working with him. I await the opportunity to continue my academic journey under his supervision.

I also gratefully acknowledge the start-up funding provided by the Faculty of Engineering at McMaster University.

Finally but not least, I would like to deeply thank my family and friends for their love, support, and encouragement along the way.

TABLE OF CONTENTS

ABSTRACT iii
ACKNOWLEDGEMENTS iv
LIST OF FIGURES vii
LIST OF TABLES ix
1. Introduction 1
1.1. Background and motivation 1
1.2. Literature review 6
1.3. Research Objectives 8
1.4. Thesis organization 9
2. Wave loads on horizontal elements. 10
2.1. Introduction 10
2.2. Wave models 12
2.2.1. Wang (1970) 12
2.2.2. Kaplan et al. (1995) 13
2.2.3. Suchithra and Koola (1995) 16
2.2.4. Bea et al. (1999) 17
2.2.5. McConnell et al. (2004) 18
2.2.6. Cuomo et al. (2007) 21
3. Methodology 23
3.1. Fragility Analysis Methodology 23
3.2. Parameterized Fragility Analysis Methodology 25
3.3. Statistical learning techniques 27
4. Results 29
4.1. Description of the structure 29
4.2. Uplift failure mode 31

4.2.1. Uplift capacity 31
4.2.2. Uplift demand 34
4.2.3. Fragility Analysis Modeling. 35
4.3. Wave load comparisons 39
4.4. Parameterized Fragility Models 58
4.4.1. Training of the parameterized fragility models 58
4.4.2. Goodness-of-fit measures 62
4.4.3. Parameterized fragility models using SLR 67
5. Discussion and Conclusions 69
5.1. Summary 69
5.2. Conclusions 69
5.3. Future Work 71
NOTATIONS 72
REFERENCES 75

LIST OF FIGURES

Figure 1. Cargo wharf (left)and LNG jetty (right). (Port of Dampier, Pilbara Ports Authority, Australia, n.d.) 2

Figure 2. Wave-in-deck loads on a pille-supported deck. From Tirindelli et al. (2003) 3

Figure 3. Puerta Maya pier (lower) and International SSA pier (upper), Cozumel, Mexico before hurricane Wilma. (https://www.viator.com, n.d.) 4

Figure 4. Puerta maya pier (left) and International SSA pier (right), Cozumel, Mexico after hurricane Wilma. (https://thisiscozumel.com, n.d.) 4

Figure 5. Definition of force parameters. Repoduced from McConnell et al. (2003) 8

Figure 6. Vertical force history on deck (units at model scale). Reproduced from Tirindelli et al. (2003) 11

Figure 7. Wave Basin test Arangement. From Wang (1970) 12

Figure 8. Airy wave definitions 15

Figure 9. Wave flume test Arrangement. Reproduced from Suchithra & Koola (1995). 17

Figure 10. Experimental set-up in the wave absorbing flume at HR Wallingford. Reproduced from Tirindelli et al. (2003) 18

Figure 11. Jetty configurations tested at HR Wallingford 19

Figure 12. Plan view of model structure. From Tirindelli et al. (2003) 20

Figure 13. Plan view of the typical pile-supported pier deck. 30

Figure 14. Elevation view (A-A' cut) of the typical pile-supported pier deck. 30

Figure 15. Geometry details of typical deck–pile connections. 31

Figure 16 Tributary areas for evaluating demand D_{uplift} 34

Figure 17 Schematic of the fragility analysis process. 38

Figure 18. Uplift fragility surface: Seaward flat deck (SF-Cuomo) 40

Figure 19. Uplift fragility surface: Seaward deck with beams (SB-Cuomo)..... 40

Figure 20. Uplift fragility surface: Internal flat deck (IF-Cuomo) 40

Figure 21. Uplift fragility surface: Internal deck with beams (IB-Cuomo)..... 40

Figure 22. Uplift fragility curve for $Z_C = -2m$ 42

Figure 23. Uplift fragility curve for $Z_C = +2m$ 42

Figure 24. Maximum difference in $pf, uplift$ between SB-Cuomo and SF-Cuomo..... 42

Figure 25. Maximum $p_{f,uplift}$ difference between McConnell and SF-Cuomo. 45

Figure 26. Maximum $p_{f,uplift}$difference between McConnell and SF-Cuomo. 45

Figure 27. Maximum $p_{f,uplift}$difference between McConnell and SB-Cuomo. 45

Figure 28. Maximum $p_{f,uplift}$difference between McConnell and SB-Cuomo. 45

Figure 29. Uplift fragility surface: Wang (1970)..... 47

Figure 30. Uplift fragility curves: $Z_C = 0m$, Wang, McConnell, Cuomo..... 47

Figure 31 Uplift fragility curves: $Z_C = 2m$, Wang, McConnell, Cuomo..... 47

Figure 32. Uplift fragility surface: Kaplan et al. (1995) 51

Figure 33 Uplift fragility curves: $Z_C = 0m$, Kaplan, McConnell, Cuomo..... 51

Figure 34 Uplift fragility curves: $Z_C = 2m$, Kaplan, McConnell, Cuomo..... 51

Figure 35. Uplift fragility surface: Suchithra and Koola (1995) (Max) 54

Figure 36. Uplift fragility surface: Suchithra and Koola (1995) (Min) 54

Figure 37. Uplift fragility curves: $Z_C = 0m$, Suchithra and Koola, McConnell, Cuomo 54

Figure 38. Uplift fragility curves: $Z_C = 2m$, Suchithra and Koola, McConnell, Cuomo 54

Figure 39. Uplift fragility surface: Bea et al. (1999) 57

Figure 40. Maximum $p_{f,uplift}$ difference between Cuomo and Bea. 57

Figure 41. Maximum $p_{f,uplift}$ difference between Bea and Suchithra and Koola (Min). 57

Figure 42 Schematic of the training process for the prameterized fragility models. 61

LIST OF TABLES

Table 1: Coefficients for predicting vertical forces - McConnell et al. (2004) 20

Table 2: Coefficients for predicting impact forces – Cuomo et al. (2007) 22

Table 3: Coefficients for predicting vertical Quasistatic forces – Cuomo et al. (2007) ... 22

Table 4 Uplift probability for $Z_C = +2m$ 43

Table 5 Maximum $p_{f,uplift}$ difference between Wang, McConnell, and Cuomo models.... 48

Table 6 Maximum $p_{f,uplift}$ difference between Kaplan, McConnell, and Cuomo models.. 52

Table 7 Maximum $p_{f,uplift}$ difference between Suchithra and Koola, McConnell, and Cuomo models 55

Table 8 Statistical properties of the predictors 60

Table 9 Confusion matrices for uplift for selected parameterized fragility models 64

Table 10 Goodness-of-fit for uplift for seaward flat deck (SF-Cuomo) 65

Table 11 Goodness-of-fit for uplift for seaward deck with beams (SB-Cuomo) 66

1. Introduction

1.1. Background and motivation

Ports have a very important role in the global economy and trade. Approximately 40% of the global population lives in close proximity to the coast (UNCTAD, 2019) and ports act as links between production activity and consumption. With approximately 85% of transported goods being shipped at some point via sea (UNCTAD, 2020), ports have consequently a huge economic importance for the local and global economy. For example, in 2018 alone, shipping was responsible for 25.7% of US GDP employing more than 650,000 people (Martin Associates, 2019).

Ports are either located in naturally protected areas or are protected by breakwater structures, providing harbor tranquility for ships to moor but also protecting structures within the harbor against hydraulic loads. Port structures typically consist of decks supported on piles, suspended above the still water level. They can have beams or attachments running underneath the deck and they are typically open, allowing water to flow freely underneath the structure. These pile-supported structures (*Figure* 1) are usually oriented parallel or perpendicular to the shoreline, and their length can vary between 0.5km – 5km (Cuomo et al. 2007). They can carry cargo conveyors to load and unload cargoes from vessels or they can be leisure and passenger terminals to allow ships to moor and load and unload passengers (typically parallel to the coastline, called wharves, piers, or jetties), or extending deep into the sea, carrying delivery lines to liquid natural or petroleum gas (LNG or LPG) terminals at the shore (typically perpendicular to the coastline, called jetties).

Figure 1. Cargo wharf (left) and LNG jetty (right). (Port of Dampier, Pilbara Ports Authority, Australia, n.d.)

However, there are occasions where such structures can be found in unprotected areas. Example of such structures can be pipe-carrying jetties, extending deep into the sea to facilitate larger LNG or LPG vessels connecting to terminals, where the construction of protective breakwater structures is uneconomical (McConnell et al. 2004). Other examples of exposed pile-supported structures include smaller regional jetties in tropical regions facilitating ferry services or provide emergency access to remote locations (McConnell et al. 2004). A common approach for protecting such exposed pile-supported structures from wave attacks which is mainly adopted by the offshore industry, is the airgap approach, where sufficient clearance is provided, typically 1.5m above the crest of the design wave (McConnell et al. 2004). But this approach cannot always be adopted since many of these structures must be low enough to allow ships to moor. Thus, decks are exposed to wave attacks resulting in horizontal, uplift and inundation loads (i.e., wave-in-deck-loads)

(Figure 2), and during hurricane events storm-induced surge can further limit this clearance exposing pile-supported decks into even larger wave-in-deck loads as the available clearance decreases (Seiffert et al. 2014). Additionally, climate change may increase the exposure of pile-supported decks to wave loads due to sea level rise (Lamberti et al. 2011).

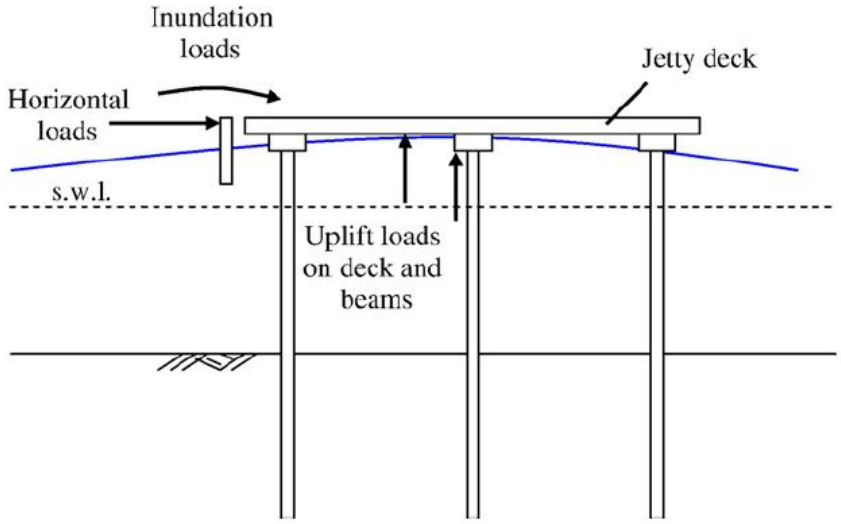

Figure 2. Wave-in-deck loads on a pille-supported deck. From Tirindelli et al. (2003)

In fact, there are many recent examples of pile-supported coastal structures being damaged during hurricanes. For example, structural damage was reported during hurricane Katrina and Wilma (2005) to pile-supported piers along Louisiana, Mississippi and Alabama coastlines (Gutierrez et al. 2006), while during hurricane Wilma (2005) wharves located at the international cruise terminal in Cozumel, Mexico (Figure 3, Figure 4) were severely damaged (Bardi et al. 2007). Also, during hurricane Sandy (2012) piers at ports in New York and New Jersey experienced severe damages (Sturgis et al. 2014). Much more recently hurricane Hanna (2020) destroyed the T-head end and unseated large portion of the deck of the Bob Hall pier at Corpus Christi, Texas (Freeman, 2020).

Figure 3. Puerta Maya pier (lower) and International SSA pier (upper), Cozumel, Mexico before hurricane Wilma. (https://www.viator.com, n.d.)

Figure 4. Puerta maya pier (left) and International SSA pier (right), Cozumel, Mexico after hurricane Wilma. (https://thisiscozumel.com, 2014)

Predicting those hydraulic loads is a complex process and several approaches have been proposed throughout the years, with significant amount of work dating as far back as the early 1950s, with most studies using both theoretical and physical models to predict and describe the loading process (Allsop et al. 2009). But despite the apparent vulnerability of exposed pile-supported deck structures to wave loading and the lack of robust guidance for estimating the wave loading (McConnell et al. 2004), little research has been done to address the impact of the uncertainties of the wave loading on the structural safety of exposed pile-supported deck structures. To explore the gaps in the risk assessment of pile-supported structures, Balomenos & Padgett (2018a) proposed a probabilistic framework for developing analytical fragility models for pile-supported wharves and piers exposed to waves and storm induced surge. Then, adopting this framework Balomenos & Padgett (2018b) provided an initial exploration into the sensitivity of the fragility estimate to epistemic uncertainties in the wave load model. Balomenos & Padgett (2018c) further explored the influence of the hazard parameter variation on the fragility estimate. Finally, Maniglio et al. (2021) proposed a methodology for developing parameterized fragility models for ports subjected to hurricane-induced storm surge and wave loading, also considering the influence of aging. Thus, the motivation of this research is to access the effect of different wave models on the uplift risk of pile-supported structures exposed to extreme coastal loads.

1.2. Literature review

A robust and accurate way for predicting those hydraulic forces is necessary for the purpose of design and producing a realistic risk assessment estimate for existing infrastructure. So far, for predicting the uplift wave forces on horizontal elements, most methods available are complex to apply without much practical guidance for their use (McConnell et al. 2004). Several approaches have been proposed, involving simplifications and mainly based on 2D assumptions (Allsop et al. 2003). Efforts to study the wave uplift forces begin as early as the early 60's. The first experimental studies of uplift forces on horizontal elements were those of El Ghamry (1963) and later Wang (1967, 1970). El Ghamry (1963) was the first to observe the uplift force as a short duration high magnitude initial peak, followed by a small magnitude long duration quasi-static component (Figure 5), where he examined breaking and non-breaking regular waves slamming on horizontal plates. Wang (1967, 1970) who performed 3D experiments on a pier model subjected to wave slamming derived a simple expression for uplift pressures. The results between the two for periodic waves were in fairly agreement. French (1969) with his laboratory studies confirmed the impulsive followed by a quasi-static component of the uplift force first observed by El Ghamry (1963) and Wang (1967, 1970). Broughton and Horn (1987) also performed physical tests, but due to low sampling rate, expressions for the slow varying quasistatic component were reported. Later Toumazis et al. (1989) and Shih & Anastasiou (1992) utilizing pressure measurements and video recordings to examine the interaction between wave crest and the structure derived equations to predict uplift forces on platform decks. Suchithra and Koola (1995) performed physical tests with and without underside beams

for various clearances to examine the influence of underside beams on the expression of the uplift force. Kaplan (1992), Kaplan et al. (1995) conducted a serries of studies on offshore platforms and proposed a semi-analytical equation by extending Morison's (1950) equations and calibrating the inertia and drag force component. Bea et al. (1999, 2001) conducted a serries of offshore experiments for the purpose of refining the guidelines of the American Petroleum Institute (API). In the experiments the primary focus was the horizontal loads on offshore platforms but an expression for vertical force was also reported. Additionally, an expression accounting for the dynamic amplification due to dynamic response of the structure was also reported.

In more recent years, attempts were made to develop analytical forms to predict wave loads on horizontal elements. Physical tests were carried out at HR Wallingford to measure wave forces on a typical exposed jetty structure to develop simplified equations for predicting the impact and quasi-static components for the wave forces for near shore structures like wharves and piers. The results from this experiment enabled McConnell et al. (2004) to propose a new prediction formula for wave forces on exposed jetties. After further analyzing the original data from the exposed jetty project, Cuomo et al. (2007) proposed a new interpretation on the prediction equations. More recently, Gaeta et al. (2012) carried out physical tests at Forschungs-Zentrum Küste (FZK) in Germany in a much bigger comparatively scale to study the effects of venting in close-to-full scale conditions.

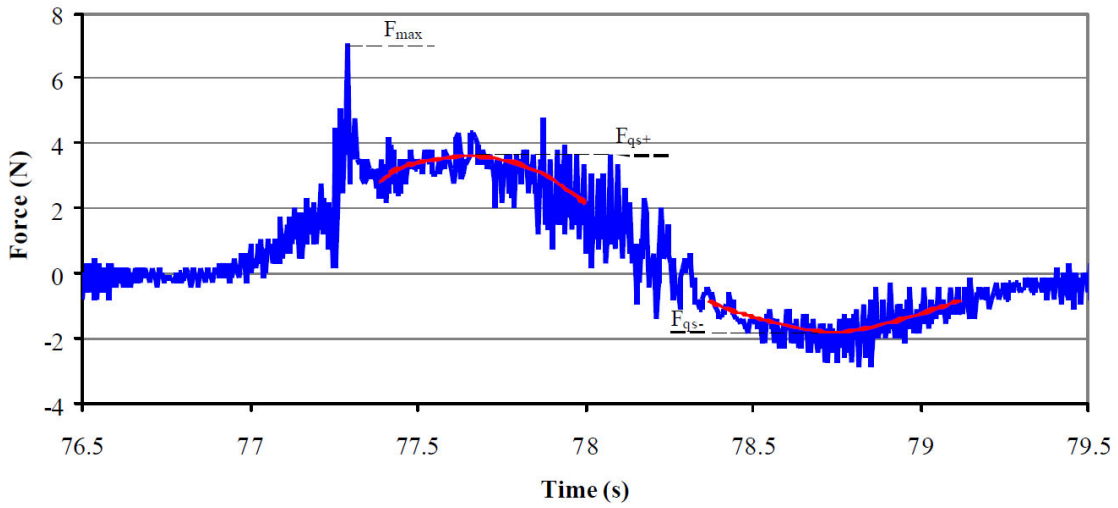

Figure 5. Definition of force parameters. Repoduced from McConnell et al. (2003)

1.3. Research Objectives

This research has four objectives. Given the number of wave models available for the purpose of estimating the uplift wave loads on pile-supported costal structures, which are either empirical in small scale experiments (e.g. , Wang (1970), McConnell et al. (2004), Cuomo et al. (2007)) or semi-empirical based on analytical expressions of wave pressures on flat plates (i.e. based on Morison's equations) and/but calibrated mainly by the offshore industry (e.g. Kaplan et al. (1995), Bea et al. (1999)), this research aims to:

- Investigate the effect of wave model selection on the estimated probability of structural damage.
- Explore the sensitivity of each wave model to selected intensity measures.
- Provide preliminary insights on the proper wave model selection.
- Develop parameterized fragility models that can enable rapid risk assessment of pile-supported ports across a region.

1.4. Thesis organization

This thesis is organized in five chapters. Chapter 1 outlines the significance of pile-supported port structures, reviews the available academic literature, and outlines the motivation and the objectives of this research.

Chapter 2 presents the wave force models adopted to determine the structural demand.

Chapter 3 presents the fragility analysis framework and the machine learning techniques for the development of the proposed parameterized fragility models.

Chapter 4 presents the case study and the results of the fragility analyses as well as key comparisons between the selected wave models, followed by a discussion on the sensitivity of each model in the selected intensity measures. Chapter 4 also presents the proposed parameterized fragility models that can enable a rapid regional risk assessment of pile-supported port structures.

Finally, Chapter 5 provides a brief summary of the current study and discusses the conclusions of this research as well as opportunities for future work.

2. Wave loads on horizontal elements.

2.1. Introduction

Wave-in-deck forces can be horizontal loads on beams, fenders or other projected elements and vertical loads (uplift or downward) on deck and beams (Allsop et al. 2003). While previous work highlighted the vulnerability of aging pile-supported piers and wharves to both horizontal and uplift loads (Maniglio et al. 2021), usually uplift forces are the most critical (Balomenos & Padgett, 2018a).

As first described by El Ghamry (1963), uplift force is characterized by an initial peak force of considerate magnitude but short in duration (impact or impulsive force), followed by a slowly varying uplift force of a lesser magnitude but considerable in duration, first positive and then negative (quasistatic or pulsating force) (Figure 6). As a wave crest propagates underneath a structure it transfers its momentum to the structure's underside, with more violent impacts having smaller time rises and longer times rises leads to smaller impacts (Cuomo et al. 2009). But due to sometimes complexity of structures' underside, a well-defined connection between the two is intricate to establish (Cornett, 2013). Protruding elements in the underside obscure the wave propagation and increase the uplift forces, yet they can sometimes allow air to get entrapped. While entrapped air in chambers formed between structural elements create buoyancy forces, entrapped air may also reduce the impact force due to wave slamming. The compression of this pocket of air leads to a "cushioning" of the wave slamming, increasing the rise-time resulting in a smaller initial impact pressure (Cuomo et al. 2009). Cuomo et al. (2009) studied extensively the role of venting openings in coastal bridges. Cuomo et al. (2009) observed that small openings to

vent the entrapped air further reduces the wave impact by damping pressure oscillations within the chamber, whilst very large openings allow air escape rapidly, reducing the cushioning effect of the air pocket. More recently, Gaeta et al. (2012) studied the effect of venting openings on a large-scale jetty experiment, also observing the cushioning effect of entrapped air. Thus, the interaction between the wave crest and the structures' underside is critical. However, since jetty like structures are being structurally less complex compared to coastal bridges, the effect of entrapped air for pile-supported ports has not been sufficiently studied (Gaeta et al. 2012). Thus, in this chapter an overview of the most important wave models for estimating vertical wave-in-deck loads for port structures is presented.

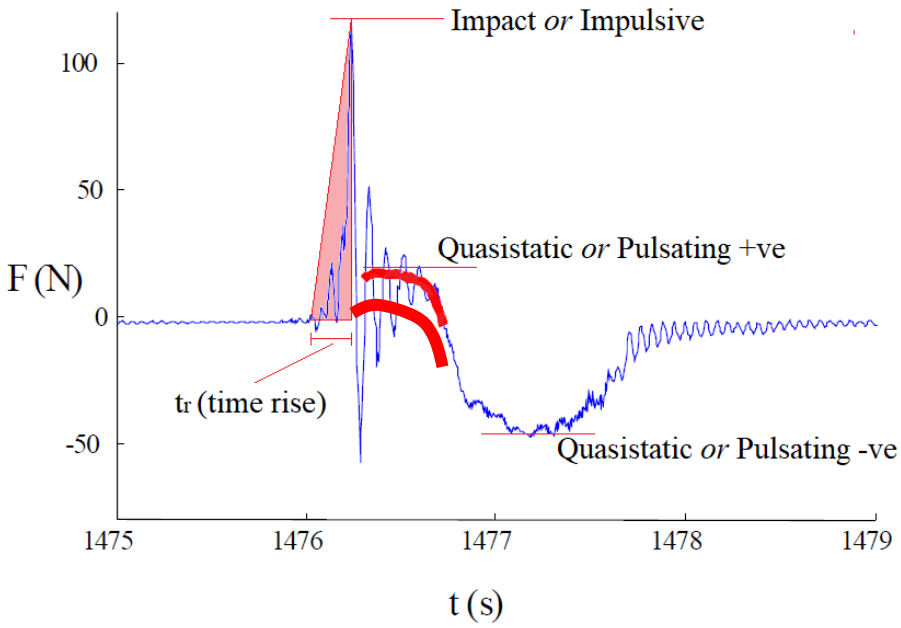

Figure 6. Vertical force history on deck (units at model scale). Reproduced from Tirindelli et al. (2003)

2.2. Wave models

2.2.1. Wang (1970)

Wang (1967, 1970) conducted physical model experiments in a wave basin at the Naval Civil Engineering Laboratory in Port Hueneme California, to study the uplift pressures of horizontal plates suspended above water. The experiments were conducted in a 27.5 m by 27.5 m square basin where pressures on a 1.8 m by 0.038 m plate were measured, originating from waves generated by a plunge opposite from the test locations within the basin (Figure 7). The plate clearances varying between 0 cm and 3.8 cm above the still water level. The wave heights had a maximum heigh of 15 cm.

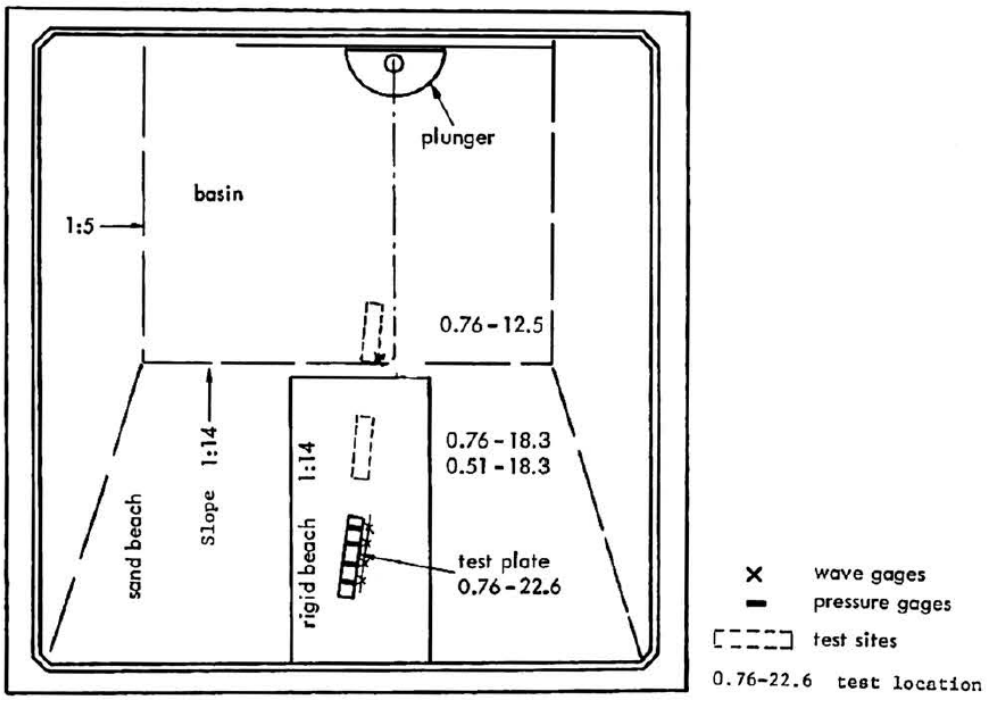

Figure 7. Wave Basin test Arangement. From Wang (1970)

Wang (1967, 1970) confirmed the observations of El Ghamry (1963) that the uplift pressures have two components, a short in duration impact pressure and a smaller in

magnitude but longer in duration quasistatic component. An empirical expression for the uplift impact pressure was presented in Wang (1970)

$$P_{v,imp} = \frac{\pi\, H_{max}\, \rho\, g}{2} \tanh\left(\frac{2\pi d_s}{L_m}\right) \sqrt{\left(1 - \frac{4Z_c^2}{H_{max}^2}\right)} \quad (1)$$

where H_{max} is the maximum wave height, ρ is the water density (taken as 1,030kg/m^3), g is the gravitational acceleration, d_s is the water depth, L_m is the wavelength, and Z_C is the deck clearance from the still water level. The wavelength $L_m$is calculated as (AASHTO, 2008)

$$L_m = \frac{g\, T_p^2}{2\pi} \sqrt{\tanh\left(\frac{4\pi^2}{T_p^2}\, \frac{d_s}{g}\right)} \quad (2)$$

where $T_p$is the wave period corresponding to H_{max}.

2.2.2. Kaplan et al. (1995)

Kaplan (1992), Kaplan et al. (1995) proposed a semi-analytical model to predict the uplift forces based on the analytical equations proposed by Morison (1950). According to Kaplan (1992), Kaplan et al. (1995), as the wave propagates underneath the deck, it transfers its energy to the deck or other protruding elements, and the time variation of the wave-in-deck loads result from the combination of an inertia force component and a drag force component. Kaplan (1992), Kaplan et al. (1995) proposed equations by experimentally determining drag and inertial force coefficients at a serries of experiments carried out at typical offshore conditions at Ekofisk field in Norway, followed by laboratory experiments. Additionally, the proposed expression considers the deck porosity and

presence of adjacent elements (i.e., cellar and scaffold decks with many crossmembers, made up of cylinders, angle sections, plates, etc. which were relatively densely distributed) to include the effect of velocity blockage and shielding (i.e., change in the wave velocity field due to the presence of adjacent elements perpendicular to the velocity direction) and include a physical explanation of various observed phenomena. It was observed that for the case of a porous grating decks, the vertical impact loads were 20-25% of those for solid decks, while horizontal loads were essentially the same regardless the deck grating.

The proposed expression for the total vertical load works through the following expression (Kaplan et al. 1995)

$$F_{V,total} = \rho \frac{\pi}{8} b_w \frac{l^2}{\left[1 + \left(\frac{l}{b_w}\right)^2\right]^{1/2}} \ddot{w} + \rho \frac{\pi}{4} b_w l \frac{dl}{dt} \frac{1 + \frac{1}{2}\left(\frac{l}{b_w}\right)^2}{\left[1 + \left(\frac{l}{b_w}\right)^2\right]^{3/2}} \dot{w} + \frac{\rho}{2} b_w l C_D \dot{w}|\dot{w}| \quad (3)$$

where ρ is the water density, b_w is the width of the examined area, l is the wetted length (Figure 8), $\ddot{w}$ is the instantaneous particle vertical acceleration at the level of contact of the wave with the deck, the term $\frac{dl}{dt}$ is equal to the wave celerity C (taken as $C = {L_m}/{T_p}$, where L_m is the wavelength and T_p is the wave period) and goes to zero after the wave crest have fully developed, $\dot{w}$ is the instantaneous vertical particle velocity and C_D is the drag coefficient (e.g., $C_D = 2.00$ for a rectangular plate (Kaplan et al. 1995)).

The particle vertical velocity $\dot{w}$, as suggested by Kaplan et al. (1995), is calculated based on linear wave theory (Airy wave) as

$$\dot{w} = \frac{H_{max} \cdot g \cdot T_p}{2 \cdot L_m} \cdot \frac{\sinh\left[2 \cdot \pi \left(\frac{d_s + z}{L_m}\right)\right]}{\cosh\left[\frac{2 \cdot \pi \cdot d_s}{L_m}\right]} \sin(k \cdot x - \omega \cdot t) \quad (4)$$

where d_s is the water depth, z is the vertical spatial coordinate of the particle measured from the still water level (s.w.l.) (*Figure 8*), k is the wave number, x is the horizontal special coordinate of the particle, ω is the wave frequency and t is the time. The particle vertical acceleration $\ddot{w}$ is calculated as

$$\ddot{w} = -\frac{g \cdot \pi \cdot H_{max}}{L} \cdot \frac{\sinh\left[2 \cdot \pi \left(\frac{d_s + z}{L_m}\right)\right]}{\cosh\left[\frac{2 \cdot \pi \cdot d_s}{L_m}\right]} \cos(k \cdot x - \omega \cdot t) \quad (5)$$

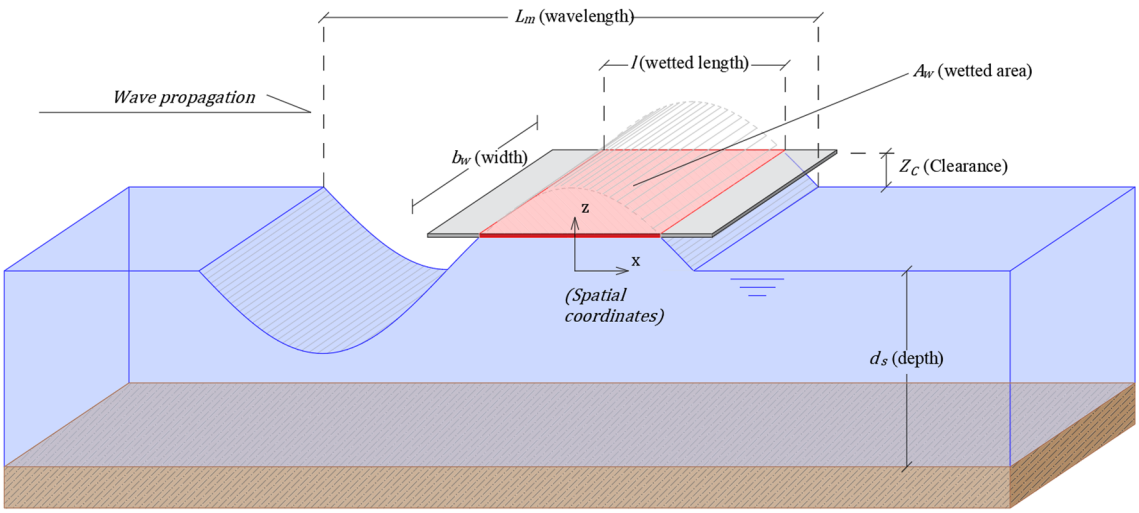

Figure 8. Airy wave definitions

2.2.3. Suchithra and Koola (1995)

Suchithra and Koola (1995) performed physical experiments to determine an expression for the uplift loads on horizontal elements as well as study the effect of underside beams on the force estimate. The experiments were conducted in the 0.3m by 10m wave flume (Figure 9) of the Ocean Engineering Centre at the IIT, Madras. A 0.25 m by 0.25 m test plate was tested, with four different configurations of underside stiffeners: no stiffeners, stiffeners in longitudinal direction, stiffeners in transverse direction, stiffeners both in longitudinal and transverse direction.

Suchithra & Koola (1995) found that the uplift force was mostly affected by the period of the incident wave and the clearance of the element, and also observed air entrapment when underside beams were presented, causing air pockets to develop and reduce the impact forces, while longitudinal beams was found to slightly increase the impact forces. An expression for the total impact force was proposed as (Suchithra and Koola, 1995)

$$F_{v,imp=\frac{1}{2}C_s \rho\, A_w \dot{w}^2} \tag{6}$$

where C_S is a slamming coefficient, ρ is the water density, A_w is the wetted area of contact ($A_w = l \cdot b_w$) and $\dot{w}$ is the instantaneous vertical velocity. The coefficient C_S was found to vary between 2.5 and 10.2 and was mainly dependent on the frequency of the incoming wave and the clearance of the element. A modified slamming coefficient $C_{ns} = C_s \cdot {}^{z}/_{L}$ (average value=1.7, where z is the deck clearance and L is the wavelength) independent of frequency was also defined and was found to decrease for increasing clearances.

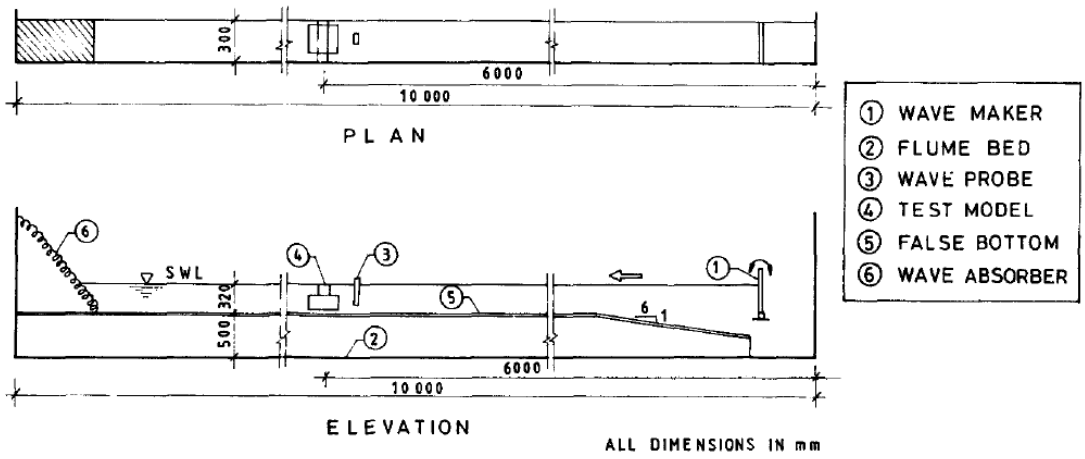

Figure 9. Wave flume test Arrangement. Reproduced from Suchithra & Koola (1995)

2.2.4. Bea et al. (1999)

Bea et al. (1999), analyzed the performance of oil platforms in the Gulf of Mexico during hurricanes, and proposed modifications to the American Petroleum Institute (API) deck wave force guidelines. The proposed formula, which was based on Morrison's Equations, was a combination of laboratory measurements and measured forces on decks. The total wave force, separated into a buoyancy, drag, lift, inertia force and a slamming force can be estimated with the following equation (Bea et al. 1999)

$$F_{v,total}=F_{boyany}+\frac{1}{2}\rho C_D A_w \dot{w}^2+\rho C_M V\,\ddot{w} \tag{7}$$

where F_{boyany} is the buoyancy force, ρ is the water density, C_d is the drag coefficient, $A_w$is the wetted area of contact, $\dot{w}$ is the maximum vertical particle velocity, C_m is the inertia coefficient, V is the volume of the deck inundated and $\ddot{w}$ is the maximum vertical particle acceleration. The coefficients C_D and C_M can be assumed as 2 and 3.5 respectively (Douglass et al. 2006).

2.2.5. McConnell et al. (2004)

Recognizing the lack of robust guidance for predicting horizontal and upward hydraulic loads on exposed pile-supported jetties, Tirindelli et al. (2003) and McConnell et al. (2003, 2004) conducted a series of small-scale laboratory experiments, where a 1 m by 1.1 m jetty was tested against irregular sea states for various wave heights and deck clearances. Tests were conducted in the absorbing flume of HR Wallingford (Figure 10). Significant wave heights were varying between 0.1 and 0.22 meters and clearances between 0.01 and 0.16 meters. The waves generated in the flume had a period ranging between 1 and 3 seconds.

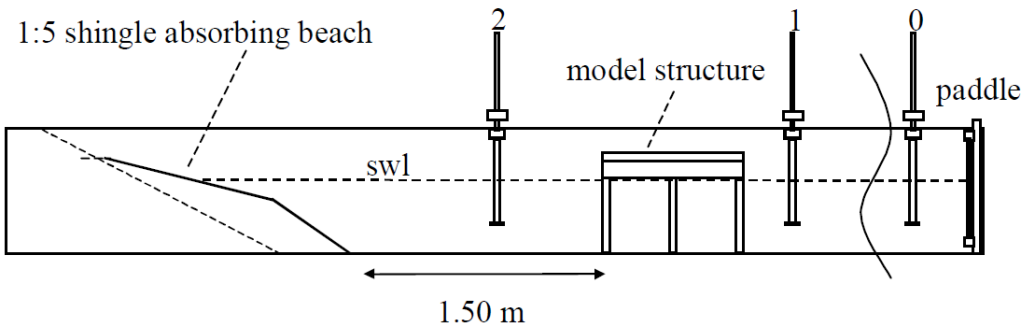

Figure 10. Experimental set-up in the wave absorbing flume at HR Wallingford. Reproduced from Tirindelli et al. (2003)

The following three jetty configurations were tested: (a) decks with flat deck underside, where waves can propagate longitudinally relatively unabstracted; (b) decks with overhang beams, where the wave crest can interfere with the propagating waves; (c) decks with overhang beams and side panels to limit the 3-dimensiaonl effects.

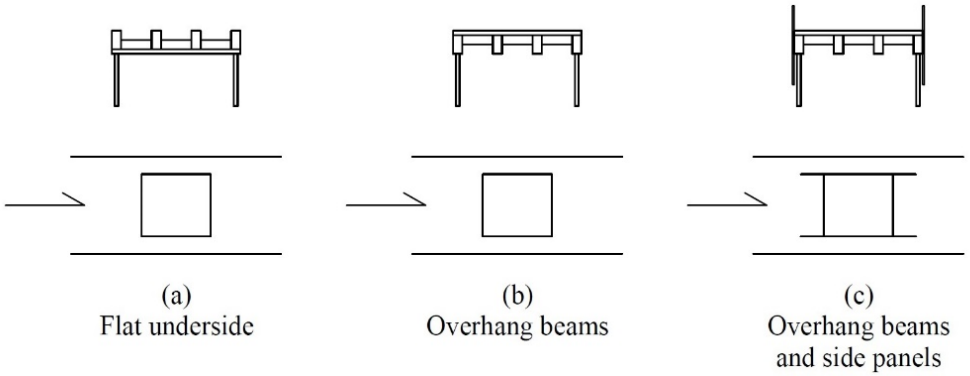

Figure 11. Jetty configurations tested at HR Wallingford

An expression for the maximum vertical force was proposed (McConnell et al. 2004)

$$F_{v,imp} = F_{v,qs} \frac{\alpha_{v,imp}}{(t_r/T_m)^{\beta_{v,imp}}} \tag{8}$$

where $\alpha_{v,imp}$ and $\beta_{v,imp}$ are coefficients for determining the vertical impact force for the examined location with respect to wave exposure (i.e. seaward or internal decks and beams, Figure 12) and are presented in Table 1, t_r is the rise time, T_m is the mean wave period and $F_{v,qs}$ is the vertical quasi-static force, determined as (McConnell et al. 2004)

$$F_{v,qs} = F_v^* \frac{\alpha_{v,qs}}{\left[\frac{\eta_{max} - z_c}{H_s}\right]^{\beta_{v,qs}}} \tag{9}$$

where $\alpha_{v,qs}$ and $\beta_{v,qs}$ are coefficients for determining the vertical quasi-static force with respect to wave exposure and are presented in Table 1, $H_s$is the significant wave height, where $H_s = H_{max}/1.8$ (AASHTO, 2008), Z_C is the vertical distance between an element and the water surface, η_{max} is the maximum crest elevation, and is calculated as (McConnell et al. 2004)

$$\eta_{max} = \frac{H_{max}}{2} exp\left(\frac{2\pi}{L_m}\frac{H_{max}}{2}\right) \quad (10)$$

and F_v^* is the vertical basic force (the hydrodynamic force at the considered element elevation) defined as

$$F_v^* = A(\eta_{max} - Z_c)\rho g \quad (11)$$

where A is the area of the examined horizontal element, ρ is the water density and g is the gravitational acceleration.

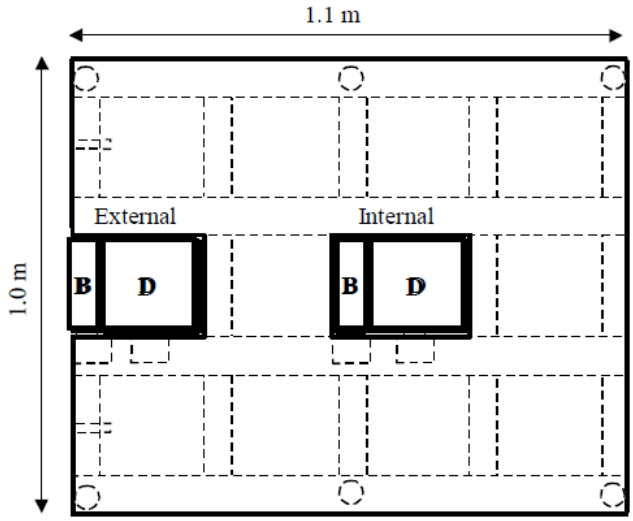

Figure 12. Plan view of model structure. From Tirindelli et al. (2003)

Table 1: Coefficients for predicting vertical forces - McConnell et al. (2004)

Examined location	$\alpha_{v,imp}$	$\beta_{v,imp}$	$\alpha_{v,qs}$	$\beta_{v,qs}$
Seaward deck	0.4 (M) or 1.00 (C)	0.7	0.82	0.61
Internal deck			0.71	0.71

Note: M = Moderate prediction; C = Conservative prediction.

2.2.6. Cuomo et al. (2007)

Cuomo et al. (2007) further examined the original data presented in Tirindelli et al. (2003) and McConnell et al. (2003, 2004), and proposed a new prediction method to refine and extend the predictions proposed originally. Cuomo et al. (2007) re-analyzed time histories of the vertical and horizontal forces using wavelet transforms, carried out further non-dimensional analysis, and account for the different structural configurations (Figure 11) in addition to the exposure conditions, i.e., seaward or internal (Figure 12), for the development of the new prediction formula. Thus, a new expression for the maximum uplift force was proposed as (Cuomo et al. 2007)

$$F_{v,imp} = \alpha_{v,imp}\, F_{v,qs} \tag{12}$$

where $\alpha_{v,imp}$ is a coefficient for calculating the vertical impact force (Table 2) and $F_{v,qs}$ is the vertical quasi-static force. For calculating the vertical quasi-static force, Cuomo et al. (2007) proposes

$$F_{v,qs} = \left[a_{v,qs} \cdot \frac{\eta_{max} - Z_c}{d_s} + \beta_{v,qs} \right] \cdot \ (\rho \cdot g \cdot \ H_s \cdot A) \tag{13}$$

where $\alpha_{v,qs}$ and $\beta_{v,qs}$ are the coefficients for the prediction of the vertical quasi-static forces (Table 3), the η_{max} is the maximum wave surface elevation, Z_C is the vertical distance between an element and the water surface, d_s is the water depth, ρ is the water density, g is the gravitational acceleration, H_s is the significant wave height and A is the area of the element exposed to the wave action.

Table 2: Coefficients for predicting impact forces – Cuomo et al. (2007)

Wave load	Configuration	Position	$\alpha_{v,imp}$
Vertical force	Flat deck	Seaward deck	2.35
Vertical force	Flat deck	Internal deck	2.35
Vertical force	Deck with beams and panels	Seaward deck	1.99
Vertical force	Deck with beams and panels	Internal deck	1.84

Table 3: Coefficients for predicting vertical Quasistatic forces – Cuomo et al. (2007)

Wave load	Configuration	Position	$\alpha_{v,qs}$	$\beta_{v,qs}$
Vertical force	Flat deck	Seaward deck	2.31	0.05
Vertical force	Flat deck	Internal deck	0.83	0.13
Vertical force	Deck with beams and panels	Seaward deck	1.23	0.51
Vertical force	Deck with beams and panels	Internal deck	0.58	0.19

3. Methodology

3.1. Fragility Analysis Methodology

Fragility analysis is a method to estimate the conditional probability of exceeding a specific limit state for given intensity measures (Balomenos & Padgett, 2018a, Balomenos et al. 2020, Maniglio et al. 2021), and thus, allowing the decoupling of the structural performance assessment from the hazard simulation (Ataei & Padgett, 2013). Fragility analysis requires the definition of a limit state function, expressed as

$$G_i(C_i, D_i) = C_i - D_i \tag{14}$$

where C_i denotes the capacity and D_i denotes the demand for the i mode of failure. Then, the fragility is expressed in terms of conditional probability as

$$p_{f,i} = P[G_i(C_i, D_i) \leq 0 \mid IMs] \tag{15}$$

where $p_{f,i}$ denotes the probability of the limit state function violation (i.e., the demand D_i exceeding the capacity C_i) for the i mode of failure and IMs are the intensity measures which the probability $p_{f,i}$ is conditioned upon. In other words, the fragility function is a mathematical function that expresses the probability that some undesirable event occurs (i.e., the i mode of failure) as a function of some measure of environmental excitation (i.e., intensity measures IMs) (Porter, 2021). Product of the fragility analysis is a 2D fragility curve where the x-axis represents the intensity measure IM and y-axis represents the probability of occurrence of an undesirable event (i.e., an i mode of failure). Namely, a fragility curve represents the cumulative distribution function (CDF) of the capacity of an

asset (i.e., strength of the structure or strength of a component of a structure) to resist an undesirable limit state (i.e., an i mode of failure) (Porter, 2021). Product of the fragility analysis can also be a 3D fragility surface when the probability of occurrence of an undesirable event is conditioned to two IMs.

The framework adopted in this research develops fragility curves based on the Monte Carlo Simulation method. The Monte Carlo Simulation method, which was first developed by Metropolis and Ulam (1949), is a computerized mathematical technique that allows to account for uncertainty by generating a number of values (i.e., simulations) for a random variable (RV) based on its statistical distribution. Therefore, a model (i.e., a mathematical function, a computational model, etc.) can be evaluated deterministically (e.g., through a limit state function) within each Monte Carlo Simulation (MCS), and uncertainty can then be propagated as the probability of a certain response for that model (e.g., number of simulations for which the limit state function is violated, over the total number of simulations).

In this study, the examined failure mode is the failure of the deck-pile connections due to vertical uplift wave loads indued by storm surge and waves. While a displacement-based limit state function would be preferable, due to lack of available data a force-based limit state function is selected. The limit state function is expressed as

$$G_{uplift}\left(C_{uplift}, D_{uplift}\right) = C_{uplift} - D_{uplift} \tag{16}$$

where C_{uplift} and D_{uplift} is the uplift capacity and the uplift demand, respectively, of the deck pile connection. The selected intensity measures are the maximum wave height H_{max}

and the deck clearance Z_C as they are the most informative parameters that affect the applied wave forces (Cuomo et al. 2007). Hence, the fragility is expressed as

$$p_{f,uplift} = P\left[G_{uplift}\left(C_{uplift}, D_{uplift}\right) \leq 0 \mid IMs\right] \quad (17)$$

where $p_{f,uplift}$ is the probability of uplift failure.

For each combination of Z_C and H_{max}, 10,000 Monte Carlo Simulations are being generated for each of the random variables involved in the calculation of the demand and the capacity, utilizing Latin Hypercube Sampling (LHS) (McKay et al. 1979). While LHS is a technique for reducing the number of simulations needed by stratifying the sample space into N intervals, and then randomly select a value from each interval such that each value has a $1/N$ probability of occurring (Nowak and Colins, 2000) contrary to the basic Monte Carlo simulation (MCS) where the sampling is random within the sampling space (i.e., "brute" MCS), LHS is used herein to efficiently sample the parameter space (Balomenos & Padgett, 2018a). Consequently, for the i^{th} simulation the demand $D_{i,uplift}$ and the capacity $C_{i,uplift}$ is calculated deterministically, and thus, the probability of uplift $p_{f,uplift}$ is evaluated as the number of violations of the limit state function (Eq. (*16*)) over the total number of simulations. The fragility surfaces are then plotted as an expression of the probability of uplift $p_{f,uplift}$ for each combination of Z_C and H_{max}.

3.2. Parameterized Fragility Analysis Methodology

As an extension to the Fragility Analysis described above, where the probability of a limit state function violation is conditioned upon a set of intensity measures IMs, in

parameterized fragility analysis the probability of a limit state function violation is also conditioned upon a set of structural parameters in order to enable risk assessment across a region (Balomenos et al. 2020). Thus, similarly to Equation ((*15*)), the parameterized fragility is expressed in terms of conditional probability as

$$p_{f,i} = P[G_i(C_i, D_i) \leq 0 \mid X, IMs] \tag{18}$$

where X is a vector of structural components (e.g., structure's geometry, material properties, etc.). Therefore, the risk estimate is not tied to a specific structure (or structural component) and fragility curves can be derived for a wide range of structures (or structural components).

Thus, the present framework utilizes parameterized fragility analysis to extend the applicability of the proposed risk assessment framework to a wide portfolio of pile-supported port structures (Maniglio et al. 2021). Utilizing Latin Hypercube Sampling (LHS) within a Monte Carlo Simulation (MCS), 10,000 random samples of uplift loads and structural parameters are created. For each Monte Carlo simulation, the violation of the limit state function (Eq. (*16*) can then be evaluated deterministically (as fail/not fail). Parameterized fragility functions are then derived by using statistical learning techniques, which are trained using the categorical results (i.e., fail/not fail) from the 10,000 Monte Carlo Simulations.

3.3. Statistical learning techniques

Several statistical learning techniques are examined in this research to develop parameterized fragility functions for the examined failure mode (i.e., uplift). Such methods are widely applied in literature, and have been used for the development of parameterized fragility functions for the regional risk assessment of bridges (Balomenos et al. 2020) and ports (Maniglio et al. 2021) subjected to storm surge and waves.

The first examined statistical learning method is the k-nearest neighbor (KNN) (Altman, 1992) which is one of the most straightforward ways for data categorization. The basic idea behind k-nearest neighbor classification method is that new objects are classified as the same class as their k-nearest neighbor objects of the training sample. For k=1, a new object is assigned to the class of its single nearest neighbor, and for k>1 the object is assigned to the class most common among its k nearest neighbors. Also, weights are assigned to the contributions of the neighbors, so that the nearer neighbors contribute more to the average than the more distant ones. Thus, for higher numbers of k, extreme values are likely to assume less importance in the prediction process.

Then, support vector machines (SVM) (Cortes & Vapnik, 1995) are examined. SVM are one of the most robust prediction methods for classification, with exceptional performance for binary classification. The objective of the support vector algorithm is to find a hyperplane in a n-dimensional space that distinctly classifies all objects while maximizing the margin distance between classes. For low-order spaces (i.e., objects with very few features) it is possible that a linear hyperplane can effectively segregate the two classes.

But for high feature spaces, a linear hyperplane cannot effectively segregate objects, thus SVM allows for higher order non-linear kernels to classify objects more effectively.

Decision trees (DT) (Breiman et al. 2017) are also examined. The decision tree algorithm utilizes a set of splitting rules to segment the feature space and based on a set of Yes/No questions (branches) predict the class of an object (leaf). Decision trees are used for both regression and classification and they are widely used for their easy to visualize decision rules. The size of the tree determines the effectiveness of prediction, with higher feature spaces requiring higher number of branches for more accurate predictions.

Finally, stepwise logistic regression (SLR) (Hosmer et al. 2013) is examined, which is commonly used for regression and classification problems due to easily interpretable results. Stepwise logistic regression is similar to multivariate linear regression; thus as a regression-based classifier, considers the probability of an object to belong into a class rather than predicting the class directly. The general form of the regression model for estimating the probability of an object to belong into a class is

$$p_f(X) = \frac{e^{(\vartheta_0+\vartheta_1 X_1+\ldots+\vartheta_P X_P)}}{1+e^{(\vartheta_0+\vartheta_1 X_1+\ldots+\vartheta_P X_P)}} \tag{19}$$

where $\vartheta_0, \vartheta_1, \ldots, \vartheta_P$ are the regression coefficients, and are estimated through maximum likelihood functions in the logarithmic space. Finally, the logit function is

$$\log\left(\frac{p(X)}{1-p(X)}\right) = \vartheta_0 + \vartheta_1 X_1 + \vartheta_2 X_2 + \ldots + \vartheta_P X_P \tag{20}$$

where $X_1, X_2, \ldots, X_P$ are the parameters of the logistic regression model.

4. Results

4.1. Description of the structure

In this research study, a typical pile-supported pier (Stringer & Harn. 2012) is selected to examine the effect of the wave model selection on the estimated probability of uplift damage on pile-supported decks. The examined pier has a total width of 30.5m, length of 39.5m, supported on 49 piles arranged in rows of 7 piles. The spacing of the piles is 6.1m in the longitudinal direction and 4.6m in the transverse direction (Figure 13). The prestressed concrete piles have a diameter of 0.61m, and the thickness of the reinforced concrete deck of the pier is 0.76 m. The deck depth (measured from the deck's underside to the seabed) is 9.1 m (Figure 14).

The pier's deck is connected to the piles using mild steel-headed dowels, which are grouted into the piles (doweled deck-pile connection), a type of connection which is commonly used for piers and wharves (Harn et al. 2010), with the dowels being anchored either bellow or above the top longitudinal reinforcement of the concrete deck (i.e., dowels anchored inside or outside of the compression zone) (ASCE 2014). Since this research study examines the effect of wave models on the risk of uplift, only the partial moment connection is examined (Figure 15), i.e., a connection commonly found in low seismicity regions, similarly to Balomenos & Padgett (2018a). The concrete cover is equal to 76mm to all faces of the pier except the top cover which is equal to 51mm (POLB, 2012). The strength of the concrete is 55 Mpa, and the yielding strength of the dowels is 414 Mpa. The spiral tie inside the pile is W20 at 51mm.

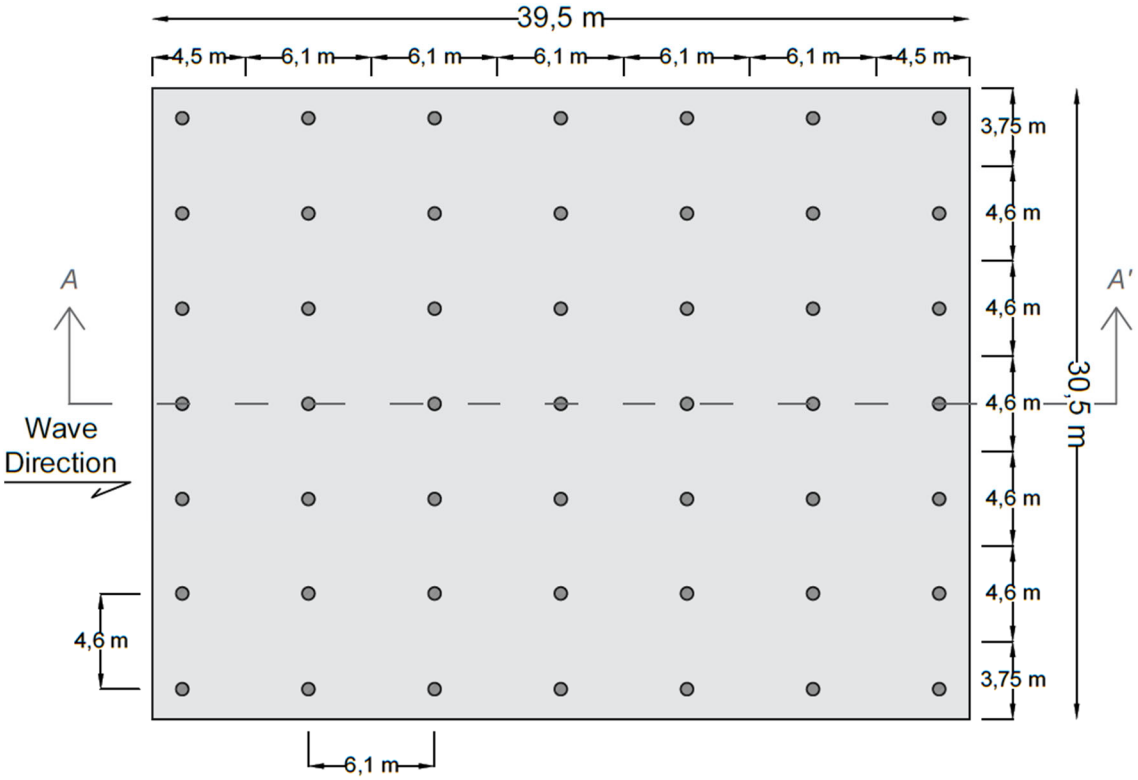

Figure 13. Plan view of the typical pile-supported pier deck.

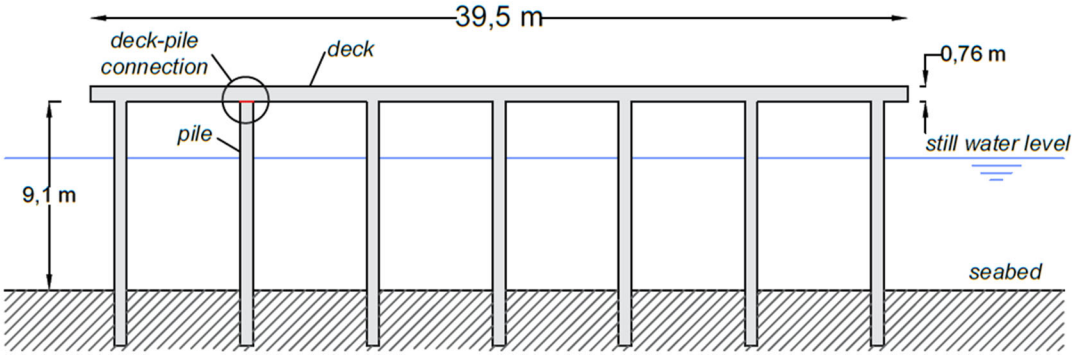

Figure 14. Elevation view (A-A' cut) of the typical pile-supported pier deck.

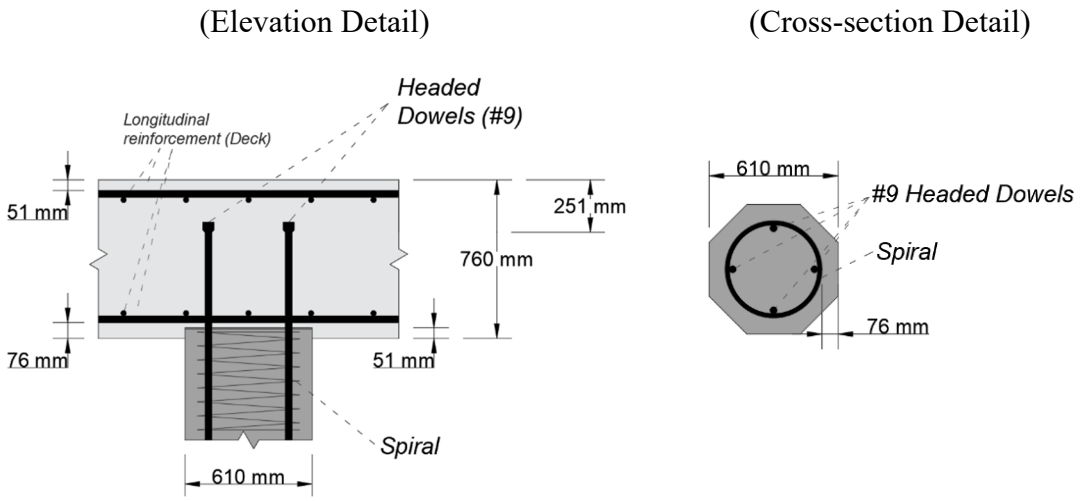

Figure 15. Geometry details of typical deck–pile connections.

4.2. Uplift failure mode

As mentioned in section 3.1, the examined failure mode is the uplift of the deck-pile connections due to vertical uplift wave loads. The limit state function (Eq. (16) requires determining the uplift capacity C_{uplift} and the uplift demand D_{uplift}, which are estimated as showing in the following sections.

4.2.1. Uplift capacity

The uplift loads of a deck-pile connection are resisted from the pullout strength of the dowelled connection, as well as the dead weight of the deck. Thus, the uplift capacity of a typical deck-pile connection is calculated as

$$C_{uplift} = F_{c,pull} + W_d \tag{21}$$

where $F_{c,pull}$ is the pull-out strength of the dowelled connection, and W_d is the weight of the deck above the connection. The weight of the deck W_d is calculated as

$$W_d = (b_w\ b_l\ b_h)\ \gamma_c \tag{22}$$

where b_w is the width of the deck, b_l is the length, b_h is the thickness and γ_c is the unit weight of the reinforced concrete.

For the pull-out strength of the dowelled connection, the strength is calculated based on the assumption that the dowels will yield, provided that there is an adequate embedment length(MacGregor & Wight. 2005). Thus, pull-out strength of the dowelled connection is calculated as

$$F_{c,pull} = n_b \times (\pi\ d_{se}\ l_{emb}\ \varphi_b) \leq n_b \times A_{se}\ f_y \tag{23}$$

where n_b is the number of dowels, d_{se} is the diameter of the dowels, l_{emb} is the embedment length of the dowels, φ_b is the bond strength, A_{se} is the cross-section area of the dowels and f_y is the yield strength of the dowels. The embedment length of the dowels is calculated as (ASCE 2014)

$$l_{emb} = \max\begin{cases} 16\ d_{se} \\ 0.3\ d_{se}\ f_y\ /\sqrt{f_c'} \end{cases} \tag{24}$$

where f_c' is the compressive strength of the concrete.

Since the bond varies along the length of the dowels anchored inside of the connection, the bond strength is calculated based on the required development length as (MacGregor & Wight. 2005)

$$\varphi_b = \frac{f_y \, d_{se}}{4 \, l_d} \tag{25}$$

where l_d is the required development length inside the connection for the dowels to develop their yield strength, and it is calculated as (ACI 2014)

$$\begin{aligned} l_d &= \left(\frac{f_y \, \psi_t \psi_e}{2.1 \, \lambda \sqrt{f_c'}} \right) d_{se} && \text{for dowels} \leq \#6 \text{ (19 mm)} \\ l_d &= \left(\frac{f_y \, \psi_t \psi_e}{1.7 \, \lambda \sqrt{f_c'}} \right) d_{se} && \text{for dowels} \geq \#7 \text{ (22 mm)} \end{aligned} \tag{26}$$

where ψ_t is a factor to account for bar placement ($\psi_t = 1$ for less than 300 mm of fresh concrete placed below horizontal reinforcement), ψ_e is a factor to account for reinforcement coating ($\psi_e = 1$ for uncoated reinforcement), λ is a modification factor to account for the reduced strength of lightweight concrete (with $\lambda = 1$ for normal-weight concrete) and $\sqrt{f_c'}$ used to calculate l_d taken not greater than 8.3 MPa.

4.2.2. Uplift demand

As described in section 2.2, the uplift loads are calculated for each wave model through Equations (*1*) to (*13*). The demand for a typical deck-pile connection can be evaluated based on the concept of tributary areas (Figure 16). A representative deck with a width of 4.6m and a length of 6.1m is examined for uplift, and for wave models that rely on the wave kinematics (i.e., Kaplan et al. (1995), Suchithra and Koola (1995), Bea et al. (1999)), a strip with an effective width of 4.6m is idealized in 2D using OpenSees (McKenna et al. 2000). There, the wave kinematics (Eq. (4) and (5)) are evaluated at their maximum at the deck level (i.e., for $\sin(k \cdot x - \omega \cdot t) = 1$ and $z = Z_C$). The wetted length is obtained by equating the expression for the wave surface elevation $\tilde{\eta}$ ($\tilde{\eta} = \frac{H_{max}}{2} cos(kx - \omega t)$) to the deck clearance Z_c.

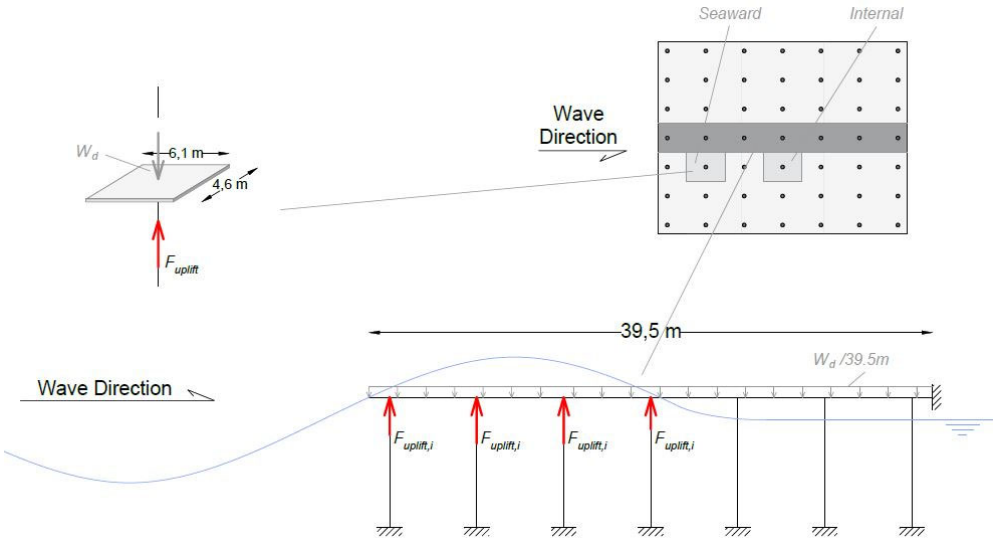

Figure 16 Tributary areas for evaluating demand D_{uplift}

4.2.3. Fragility Analysis Modeling.

While some parameters involved in the evaluation of the analytical expression of the demand D_i and capacity C_i can be assumed as deterministic (e.g., the diameter of the dowels), others may be assumed to be random variables, following a probability distribution function (e.g., the yielding strength of the dowels). Thus, as previously mentioned in mentioned in section **Error! Reference source not found.**, for each combination of the intensity measures H_{max} and Z_C, a Monte Carlo simulation is adopted, in which the Latin Hypercube sampling is used to effectively sample the parameter space to generate 10,000 samples for each random variable involved in the calculations for evaluating the structural demand and capacity. Hence, the probability of uplift for a combination of the intensity measures H_{max} and Z_C is evaluated as the number of limit-state function violations (i.e., $C_{uplift} - D_{uplift} \leq 0$) over the total number of simulations.

For modeling the uplift demand, the wave period T_p corresponding to H_{max} is considered a random variable, and it is calculated using the Longuet-Higgins (1983) joint probability of wave height and wave period as

$$f(\xi,\eta) = L(\xi/\eta)^2 \exp\left\{-\frac{\xi}{2}\left[1+\left(1-\frac{1}{\eta}\right)^2\frac{1}{v^2}\right]\right\} \tag{27}$$

where L is a constant, calculated as

$$L = [1+(v^2/4)]\left(1/\sqrt{2\pi v}\right) \tag{28}$$

ξ is the dimensionless wave height, calculated as

$$\xi = H/\sqrt{m_0} \tag{29}$$

η is the dimensionless wave period, calculated as

$$\eta = T_p/T_m \tag{30}$$

v is the bandwidth of the wave spectral density, and during the storm surge, can be assumed to be 0.3 (Massel, 1996), m_0 is the first spectral moment calculated as (Sorensen, 1993)

$$m_0 = (H_s/4)^2 \tag{31}$$

The upper bound of T_p is taken as $100\%T_m$, and the lower bound as $90\%T_m$, where T_m is the mean wave period (Longuet-Higgins 1983). The mean wave period T_m, is assumed to be 6 seconds, aligned with periods reported at locations near the shore during hurricanes Katrina and Rita (Dietrich et al. 2011) and hurricane Ike (Bender et al. 2013). Additionally, since the most realistic values of maximum impact corresponds to a dimensionless time-rise ranging between 0 and 0.1 (McConnell et al. 2004), the latter is also considered as a uniform variable ranging from 0 to 0.1. Finally, a model error term ε was introduced to account for the inherent epistemic uncertainties in calculating the uplift force. For the wave models that no error was reported, it was considered as normally distributed random variable, with a mean of 1 and a coefficient of variation (COV) of 0.1, and for the Cuomo et al. (2007) wave model the error was adopted from Cuomo et al. (2007).

For modeling the uplift capacity, the capacity of the typical dowelled connection to resist uplift loads comes from both the pull-out strength of the dowelled connection and the weight of the deck, and thus, uncertainties related to variables involved in both are propagated in the Monte Carlo simulation. More specifically, to account for construction variability, the deck thickness b_h is considered as uniformly distributed, with an upper limit

of 105% and a lower limit of 95% of the nominal, as-built plan thickness (Ataei & Padgett, 2013), while the unit weight of the concrete γ_c is considered as normally distributed, with a mean of 24kN/m^3 and coefficient of variation (COV) of 0.04 (JCSS 2001). The strength of concrete f_c' is considered normally distributed, with a mean of 55MPa and a COV of 0.09 (Nowak et al. 2011), and a lognormal distribution is adopted for the strength of steel f_y, with a mean of 414MPa and a COV of 0.04 (Nowak and Szerszen, 2003).

Thus, for each combination of Z_C and H_{max}, a sample of 10,000 values for T_p is generated. Then, for each value of T_p, the wavelength L_m is calculated (Eq. (2), followed by the maximum crest elevation η_{max} calculation (Eq. (10). Consequently, for each of the 10,000 sets of the wave parameters (i.e., T_p, L_m and η_{max}) the uplift demand is then evaluated deterministically through the equations for the uplift force as described in section 2.2 and multiplied by the model error term ε (e.g., through Eq. (12) & (13) for the Cuomo et al. (2007) wave model). Similarly, a sample of 10,000 values for each of the structural parameters (i.e., b_h, f_c', γ_c and f_y) is generated, and for each set of parameters the capacity of the connection is evaluated deterministically via Eq. (21) to (26). The probability of uplift for each combination of the intensity measures is then evaluated. Finally, the fragility surface is plotted by populating the intensity measures' space (i.e., all combinations of Z_C and H_{max}) with the corresponding probability of uplift $p_{f,uplift}$. A schematic of the process described above is presented in Figure 17.

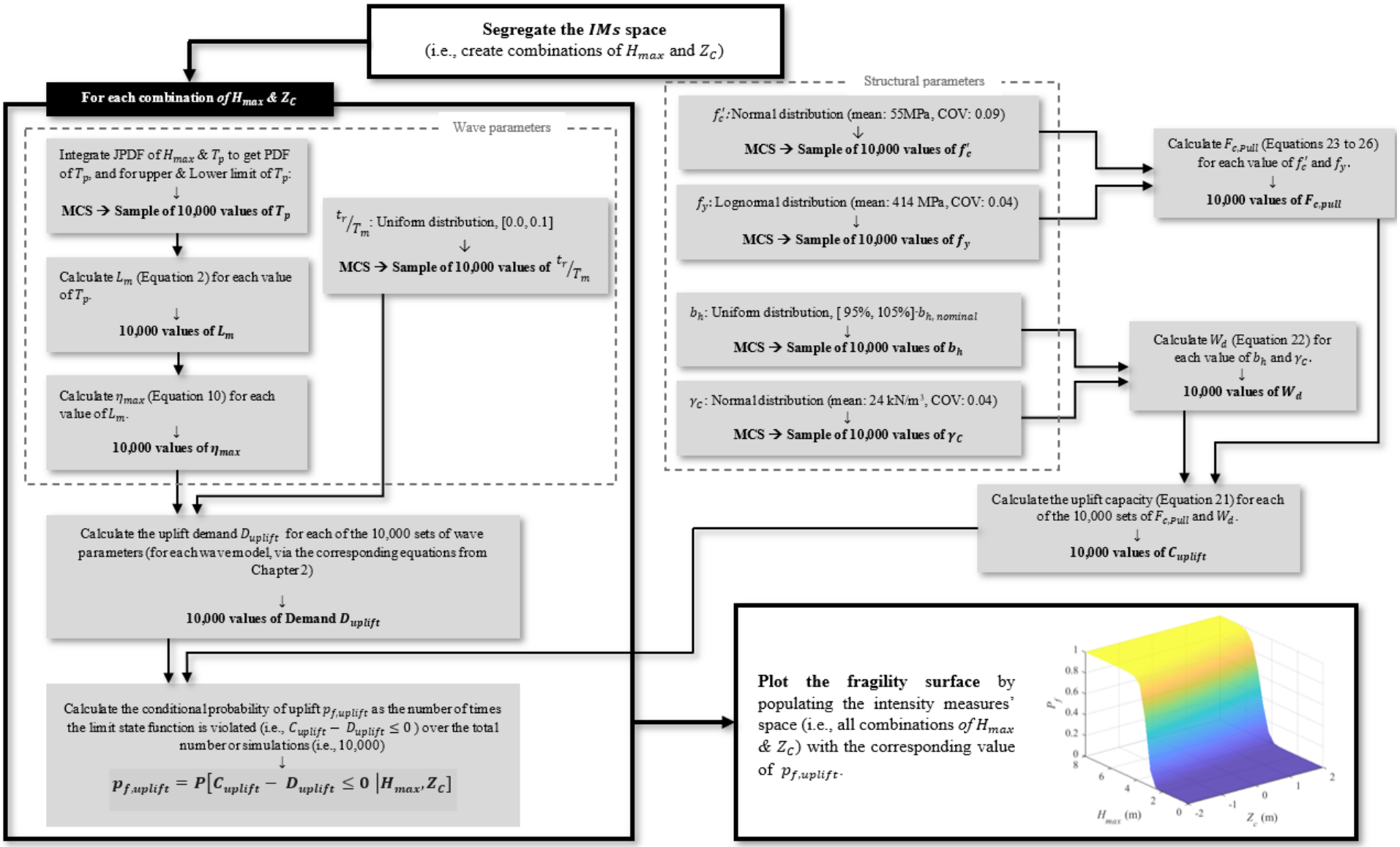

Figure 17 Schematic of the fragility analysis process.

4.3. Wave load comparisons

As mentioned earlier, a well-defined interaction between the deck's underside with the wave crest of the oncoming waves is difficult to establish (Cornett, 2013), and researchers tried to tackle this in various ways. For example while Wang (1970) considered a flat plate in his experiments, Kaplan et al. (1995) considered different cases of deck porosity and the presence or not of adjacent elements to capture their impact on wave kinematics. Also, Suchithra & Koola (1995) considered different configurations of underside stiffeners. Finally, McConnell et al. (2004) and Cuomo et al. (2007) considered cases with or without overhang beams. But since Cuomo et al. (2007) provides predictions that distinguish between the two, these two cases were considered separately; one case considering that the underside deck is flat (F) and one case where beams are running below the deck (B). For each of these two cases, two typical positions of the deck are examined, a seaward deck (S) and an internal deck (I). Therefore, four deck configurations are examined in total, i.e.: seaward flat deck (SF-Cuomo), seaward deck with beams (SB-Cuomo), internal flat deck (IF-Cuomo), internal deck with beams (IB-Cuomo).

The results indicate that seaward pile-supported decks without (Figure 18) or with (Figure 19) underside beams have higher probability of uplift failure compared to internal pile-supported decks without (Figure 20) or with (Figure 21) underside beams. Additionally, the fragility surfaces reveal a sharp transition from $p_f \cong 0$ to $p_f \cong 1$ for the seaward decks that agree with the results presented in Balomenos & Padgett (2018a) for the seaward deck using the McConnell et al. (2004) wave model. On the other hand, the fragility surfaces reveal a smooth transition from $p_f \cong 0$ to $p_f \cong 1$ for the internal decks, indicating that

uncertainty in capacity and demand parameters for the internal decks' calculations will render a smoother transition from survival to failure compared to the seaward decks' calculations no matter the presence or not of the underside beams.

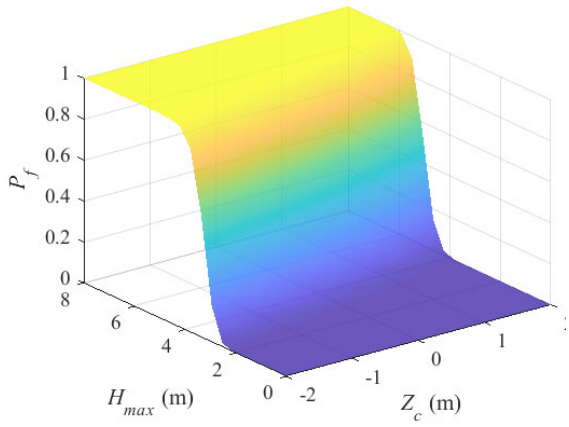

Figure 18. Uplift fragility surface: Seaward flat deck (SF-Cuomo)

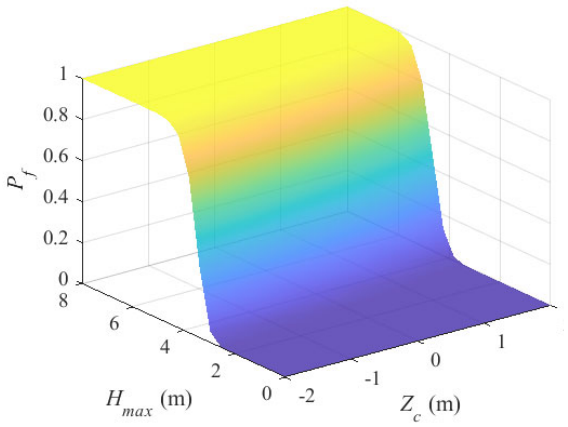

Figure 19. Uplift fragility surface: Seaward deck with beams (SB-Cuomo)

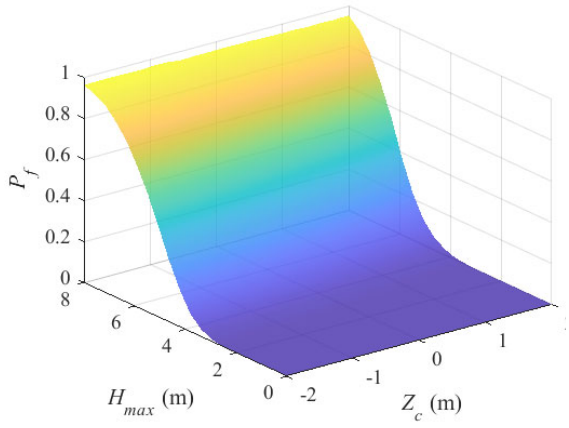

Figure 20. Uplift fragility surface: Internal flat deck (IF-Cuomo)

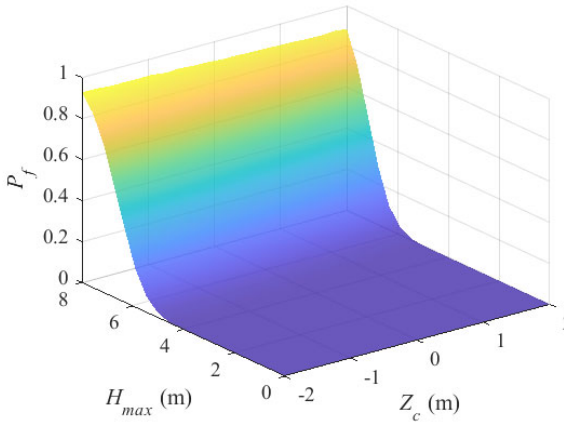

Figure 21. Uplift fragility surface: Internal deck with beams (IB-Cuomo)

Additionally, the fragility curves indicate that seaward decks with beams are less sensitive to changes in clearance compared to seaward flat decks. For example, for a 4.22 m wave height, there is a 94.31% probability of uplift for a 2 m submerged seaward deck with beams (SB-Cuomo) (Figure 22), and that probability decreases to 12.98% when the water is 2 m below the deck (Figure 23). Similarly, for a 4.22 m wave height, there is a 98.32% probability of uplift for a 2 m submerged seaward flat deck with (SF-Cuomo) (Figure 22), and that probability decreases to 1.92% when the water is 2 m below the deck (Figure 23). Thus, the uplift fragility of the decks with underside beams is less sensitive to changes in clearance. This is expected because as the clearance increases, the uplift load reduces slower for decks with underside beams since underside beams comes in contact with the wave crest, and the water gets trapped between these beams. Furthermore, the presence of underside beams increases the probability of uplift for decks above water. For example, for a 5.06 m wave height, a deck with beams 2 m above water has an 80.48% probability of uplift, and this probability reduces to 54.48% for a flat deck (Table 4). This probability difference between the two configurations can reach up to 31.57% (Table 4) when the water level is 2 m below the deck, and this maximum difference reduces linearly for the decrease of clearance (Figure 24). For the examined case study (i.e., water depth, crest elevations and clearances examined), the two predictions converge when the water level is almost at the level of the deck, e.g., 5.01% for the water level 0.11 m below deck (Figure 24), and extending for submerged decks, that difference can reach up to 26.18% for 2 m submerged decks (Figure 24) (with the negative values in Figure 24 denoting that flat decks have a higher probability of uplift).

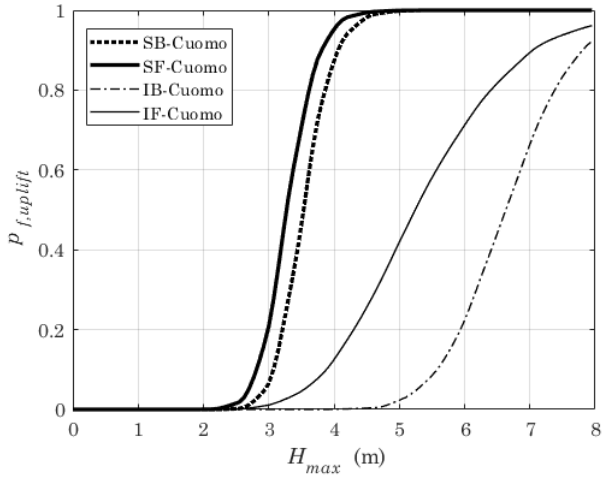

Figure 22. Uplift fragility curve for $Z_C = -2m$

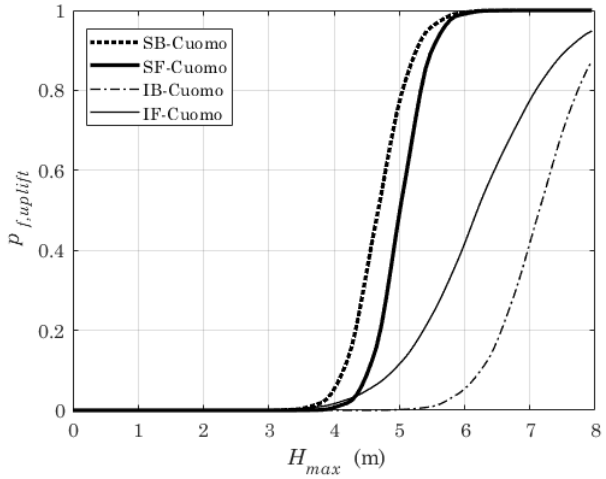

Figure 23. Uplift fragility curve for $Z_C = +2m$

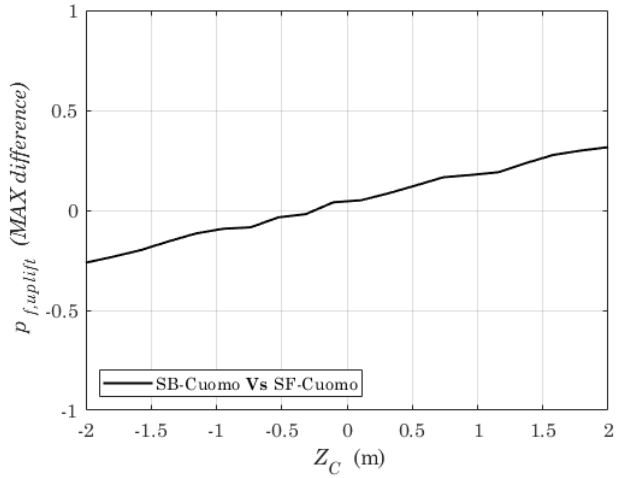

Figure 24. Maximum difference in $p_{f,uplift}$ between SB-Cuomo and SF-Cuomo

Table 4 Uplift probability for $Z_C = +2m$

H_{max} (m)	$p_{f,uplift}$		$p_{f,uplift}$
	SB	SF	(Difference)
0.01	0.00%	0.00%	0.00%
0.43	0.00%	0.00%	0.00%
0.85	0.00%	0.00%	0.00%
1.27	0.00%	0.00%	0.00%
1.69	0.00%	0.00%	0.00%
2.11	0.00%	0.00%	0.00%
2.53	0.00%	0.00%	0.00%
2.95	0.00%	0.00%	0.00%
3.37	0.15%	0.01%	0.14%
3.79	1.80%	0.10%	1.70%
4.22	12.98%	1.92%	11.06%
4.64	46.65%	15.08%	31.57%
5.06	80.48%	54.48%	26.00%
5.48	95.69%	89.23%	6.46%
5.90	99.24%	98.74%	0.50%
6.32	99.94%	99.89%	0.05%
6.74	100.00%	99.98%	0.02%
7.16	100.00%	100.00%	0.00%
7.58	100.00%	100.00%	0.00%
8.00	100.00%	100.00%	0.00%

Note: SB=SB-Cuomo; SF=SF-Cuomo.

For the case of the pile-supported deck without underside beams (i.e. flat deck) the results indicate that a higher probability of uplift is expected using the McConnell et al. (2004) model compared to the estimated probability of uplift using the Cuomo et al. (2007) model. The maximum difference in the uplift probability between the two wave models varies linearly, reaching up to 89.52% and 74.28% for a 2 meter submerged deck adopting conservative and moderate prediction respectively, and is reduced to 74.45% and 57.16% when the water is 2 meters below the deck (Figure 25). However, for the same wave height, the results agree that a maximum difference in the uplift probability is expected to be higher using the conservative coefficients in the McConnell et al. (2004) model compared to the maximum difference in the uplift probability using the moderate coefficients in the McConnell et al. (2004) model, i.e., using McConnel (C) versus McConnel (M), respectively (Figure 26). Additionally, the maximum difference in the uplift probability between the two models reach its highest value of 89.52% for a 2.53 m wave height, decreases to 74.45% for a 4.63 m wave height and then decreases rapidly (Figure 26). For the case of the pile-supported deck with underside beams, the maximum difference in the uplift probability between the McConnell et al. (2004) model and the Cuomo et al. (2007) model is reduced almost linearly with the increase of the clearance (Figure 27). For a 2 m submerged deck, the maximum difference can reach up to 92.38% considering a conservative prediction and 83.57% considering moderate prediction. For a deck 2 m above water level, the maximum difference can reach up to 43.89% and 25.90% considering a conservative and moderate prediction respectively. Similarly to the flat deck, the maximum difference in the uplift probability between the two models change for different wave

heights (Figure 28). But the maximum difference in the uplift probability has a peak of 92.45% for a 2.95 m wave height for a conservative prediction (and 83.75% for a moderate prediction), and a sudden drop, indicating a more similar behavior between the two models.

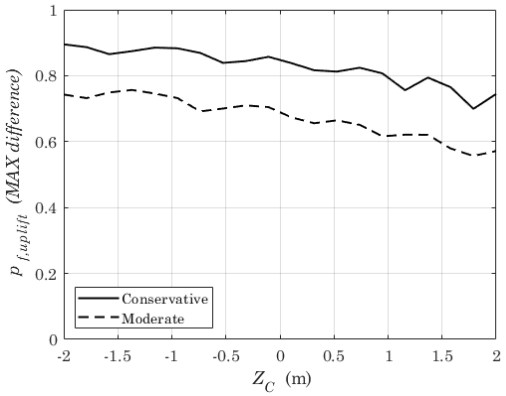

Figure 25. Maximum $p_{f,uplift}$ difference between McConnell and SF-Cuomo.

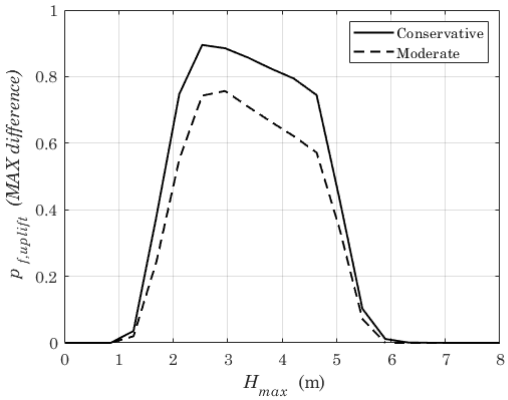

Figure 26. Maximum $p_{f,uplift}$ difference between McConnell and SF-Cuomo.

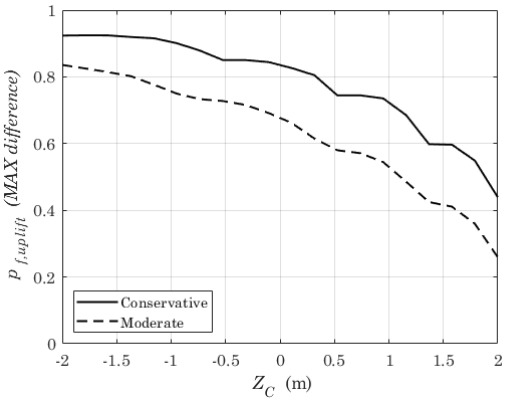

Figure 27. Maximum $p_{f,uplift}$ difference between McConnell and SB-Cuomo.

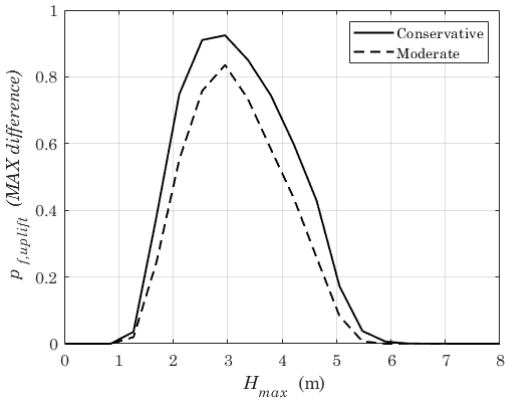

Figure 28. Maximum $p_{f,uplift}$ difference between McConnell and SB-Cuomo.

Wang (1970) model does not account for inundated decks, and models relying on wave kinematics (i.e., Kaplan et al. (1995), Suchithra and Koola (1995), Bea et al. (1999) assume that the incident wave field is not greatly affected by the structure (Morison et al. 1950), a condition which is violated for submerged decks. Thus, for those models, fragility analysis is conducted for water levels up to the deck's level (i.e., $Z_C = 0m$).

Adopting the Wang (1970) model (Figure 29) it is observed that for small clearances the uplift probability estimates are close to those derived adopting the McConnell et al. (2004) model, while as the clearance increases, the uplift probability estimates are close to those derived adopting the Cuomo et al. (2007) model. For example, for a deck at the water level subjected to a 3.37 m wave height, there is a 98.64% probability of uplift for the Wang (1970) model. The same probability is 90.26% and 73.46% for the McConnell et al. (2004) model for a conservative and moderate prediction, respectively (Figure 30). For a deck 2 m above the water level subjected to 5.05 m wave height, there is a 47.43% probability of uplift for the Wang (1970) model, 54.48% for a flat deck (SF-Cuomo) and 81.18% for a deck with beams (SB-Cuomo) (Figure 31). The maximum difference in the uplift probability between the Wang (1970) model and the Cuomo et al. (2007) model is rapidly reduced with the decrease of the water level. For example, for a deck at the water level the maximum difference in the uplift probability between the Wang (1970) model and the Cuomo et al. (2007) model is 92.93% for a deck with beams and 93.69% for a flat deck, while for a deck 2 m above the water the same maximum differences are reduced to 45.87% and 15.08% (Table 5). On the other hand, for a deck at the water level, the maximum difference in the uplift probability between the Wang (1970) model and the McConnell et

al. (2004) model is 29.74% and 25.18% for a conservative and moderate prediction respectively (Table 5). For a deck 2 m above water level the maximum difference between Wang (1970) and McConnell et al. (2004) is 88.56% for a conservative and 72.90% for a moderate prediction (Table 5).

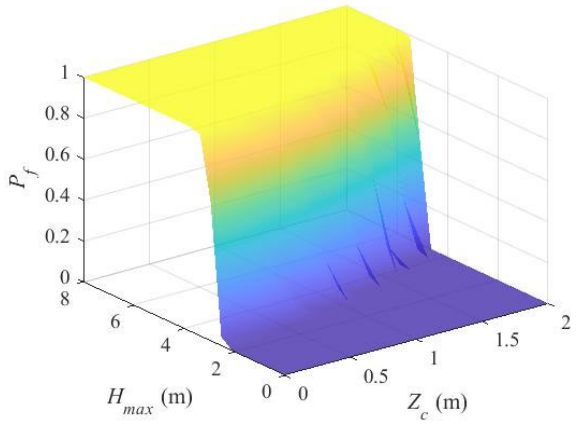

Figure 29. Uplift fragility surface: Wang (1970)

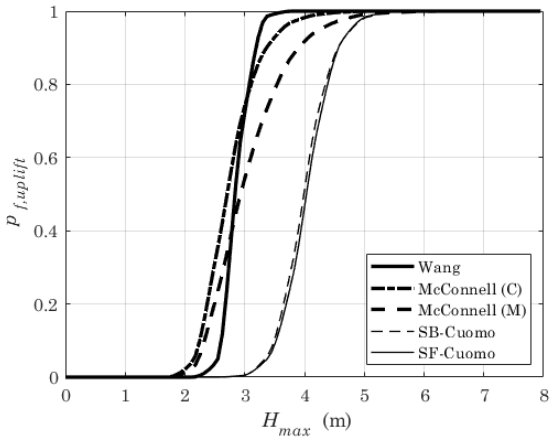

Figure 30. Uplift fragility curves: $Z_C = 0m$, Wang, McConnell, Cuomo

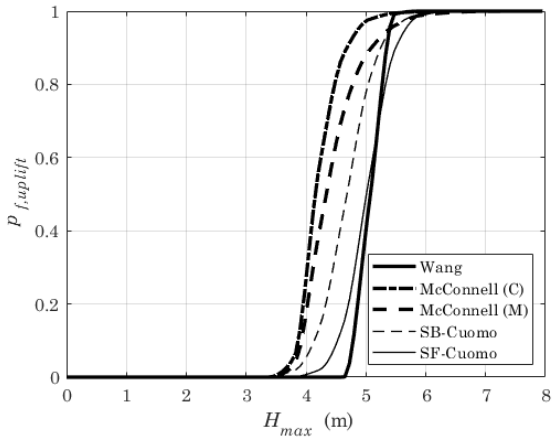

Figure 31 Uplift fragility curves: $Z_C = 2m$, Wang, McConnell, Cuomo

Table 5 Maximum $p_{f,uplift}$ difference between Wang, McConnell, and Cuomo models

Z_C (m)	Cuomo-Wang		McConnell-Wang	
	SB	SF	C	M
0.00	92.93%	93.69%	29.74%	25.18%
0.11	93.52%	93.91%	23.83%	27.03%
0.21	93.00%	94.61%	19.39%	29.82%
0.32	92.31%	93.71%	15.13%	31.21%
0.42	90.72%	92.11%	12.88%	33.26%
0.53	86.86%	88.43%	17.54%	32.22%
0.63	83.34%	90.41%	23.13%	29.85%
0.74	83.79%	91.27%	22.35%	26.63%
0.84	83.27%	91.00%	17.37%	27.52%
0.95	79.45%	86.85%	32.46%	25.29%
1.05	68.48%	79.03%	41.42%	25.70%
1.16	62.24%	81.05%	36.23%	23.20%
1.26	61.12%	79.98%	49.84%	30.53%
1.37	48.36%	68.02%	61.12%	42.63%
1.47	33.21%	59.05%	56.22%	38.71%
1.58	31.25%	59.40%	71.37%	53.15%
1.68	19.87%	42.13%	78.76%	59.86%
1.79	25.30%	31.58%	73.49%	54.02%
1.89	48.02%	24.18%	89.87%	74.09%
2.00	45.87%	15.08%	88.56%	72.90%

Note: SB=SB-Cuomo; SF=SF-Cuomo; C=McConnell (C); M=McConnell (M).

Adopting the Kaplan et al. (1995) model, the results suggest that the surge elevation will not substantially affect the uplift probability for different wave heights (Figure 32). This might happens because the examined pile-supported deck has a length smaller than the examined wavelengths (i.e. assuming a sinusoidal wave surface elevation from linear wave theory, the wave crests wet almost half of the wharf underside with the wetted length being over three times larger than the longitudinal spacing of the piles), thus changes in the wetted length due to change in clearance will not significantly affect the uplift force distribution at deck pile connections for the examined range of clearances. Furthermore, because, the Kaplan et al. (1995) model was developed for offshore platforms with large clearances and relatively unobstructed wave propagation underneath the structure, it may not effectively capture local amplification of pressures due to wave crests trapped underneath a structure near the sea water level (Cuomo et al. 2007)). Therefore, for decks near the water level, the Kaplan et al. (1995) model provides smaller uplift probability estimates compared to the McConnell et al. (2004), Cuomo et al. (2007) and Wang (1970) models, with the maximum differences reducing for larger clearances. For a deck at the water level, the maximum difference in the uplift probability between the Kaplan et al. (1995) model and the Cuomo et al. (2007) model is 83.72% for a seaward deck with beams and 83.75% for a seaward flat deck, while for a deck 2m above the water the same maximum differences are reduced to 58.98% and 32.28% (Table 6). For the deck at the water level, the maximum difference in the uplift probability between the Kaplan et al. (1995) model and the McConnell et al. (2004) model is 99.07% and 94.64% for a conservative and moderate prediction, respectively (Table 6). For a deck 2 m above water level that difference reduces to 88.56%

for a conservative and 72.90% for a moderate prediction (Table 6). For example, for a deck at the water level subjected to a 4.64 m wave height, there is a 8.44% probability of uplift for the Kaplan et al. (1995) model. The same probability is 99.75% and 97.69% for the McConnell et al. (2004) model for a conservative and moderate prediction respectively, and 92.15% for a seaward flat deck (SF-Cuomo) and 92.12% for a seaward deck with beams (SB-Cuomo) (Figure 33). For a deck 2 m above water level subjected to 5.48 m wave height, the probability of uplift is 82.61% for the Kaplan et al. (1995) model, 99.46% and 96.03% for the McConnell et al. (2004) model for a conservative and moderate prediction respectively and 89.23% for a seaward flat deck (SF-Cuomo) and 95.85% for a seaward deck with beams (SB-Cuomo) (Figure 34).

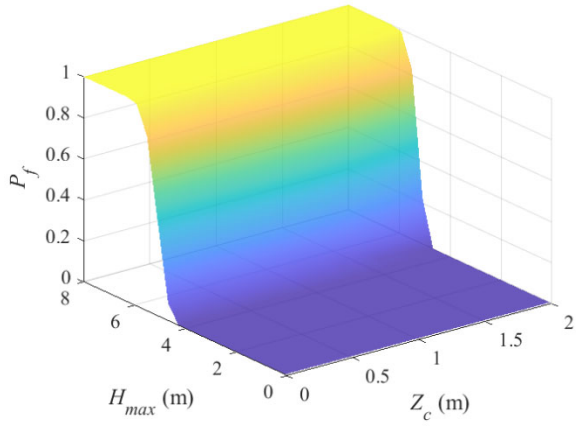

Figure 32. Uplift fragility surface: Kaplan et al. (1995)

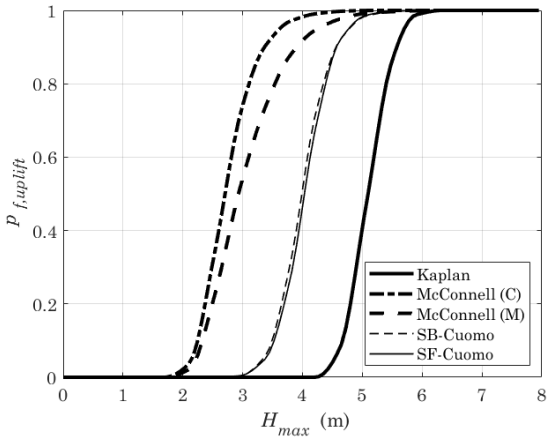

Figure 33 Uplift fragility curves: $Z_C = 0m$, Kaplan, McConnell, Cuomo

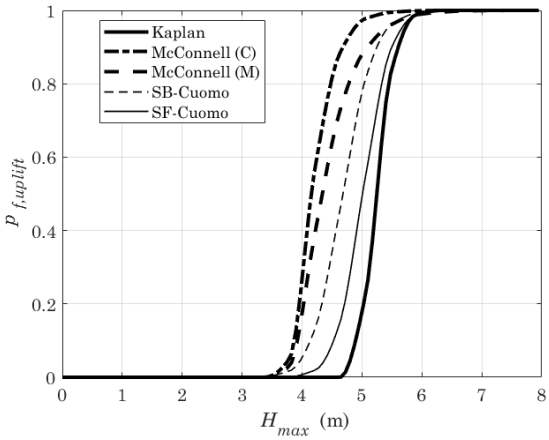

Figure 34 Uplift fragility curves: $Z_C = 2m$, Kaplan, McConnell, Cuomo

Table 6 Maximum $p_{f,uplift}$ difference between Kaplan, McConnell, and Cuomo models

Z_C (m)	Cuomo-Kaplan		McConnell-Kaplan	
	SB	SF	C	M
0.00	83.72%	83.75%	99.07%	94.64%
0.11	81.40%	80.26%	99.08%	93.89%
0.21	80.78%	79.58%	98.76%	92.97%
0.32	79.57%	77.24%	97.78%	91.77%
0.42	75.83%	72.57%	97.97%	90.58%
0.53	74.49%	70.20%	97.76%	89.89%
0.63	73.53%	66.97%	97.38%	88.63%
0.74	71.79%	63.08%	96.69%	86.87%
0.84	68.82%	57.42%	96.16%	85.48%
0.95	68.50%	55.90%	95.48%	83.72%
1.05	67.75%	52.07%	94.25%	82.53%
1.16	63.78%	46.09%	93.11%	80.20%
1.26	65.13%	42.93%	91.60%	82.85%
1.37	60.65%	37.48%	90.34%	81.24%
1.47	59.17%	33.51%	90.74%	80.90%
1.58	59.09%	30.94%	94.00%	82.38%
1.68	56.23%	31.60%	92.85%	80.37%
1.79	52.62%	32.64%	92.26%	78.71%
1.89	55.43%	33.24%	91.53%	75.75%
2.00	58.98%	32.28%	88.56%	72.90%

Note: SB=SB-Cuomo; SF=SF-Cuomo; C=McConnell (C); M=McConnell (M).

The uplift fragility surface adopting the Suchithra and Koola's (1995) model shows low sensitivity to surge elevation (Figure 35, Figure 36), similar to the uplift fragility surface derived using the Kaplan et al. (1995) model. This can be attributed to the slamming coefficient, whose value decreases for increasing clearances. Adopting the most conservative slamming coefficient (i.e., $C_S = 10.2$), the uplift probability for a pile-supported deck near the sea water level (Figure 37) is comparable to the Cuomo et al. (2007) model and lower compared to McConnell et al. (2004). For example, for water levels close to the level of the deck, the maximum difference in the uplift probability between the Suchithra and Koola (1995) model and the Cuomo et al. (2007) model is 16.38% for a seaward deck with beams (SB-Cuomo) and 20.34% for a seaward flat deck (SF-Cuomo). The same maximum difference in probability between the Suchithra and Koola (1995) model and the McConnell et al. (2004) model is 90.26% for a conservative and 73.46% for a moderate prediction, respectively (Table 7). For a deck 2 m above the water level, the Suchithra and Koola (1995) model (for $C_S = 10.2$) is the most conservative (Figure 38), with a maximum difference between that and McConnell et al. (2004) of 17.30% for a conservative and 26.10% for a moderate prediction. The same maximum difference between Suchithra and Koola (1995) and Cuomo et al. (2007) is 53.13% for a deck with beams and 83.92% for a flat deck (Table 7).

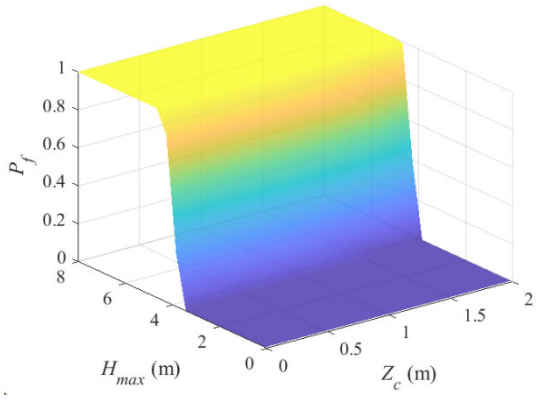

Figure 35. Uplift fragility surface: Suchithra and Koola (1995) (Max)

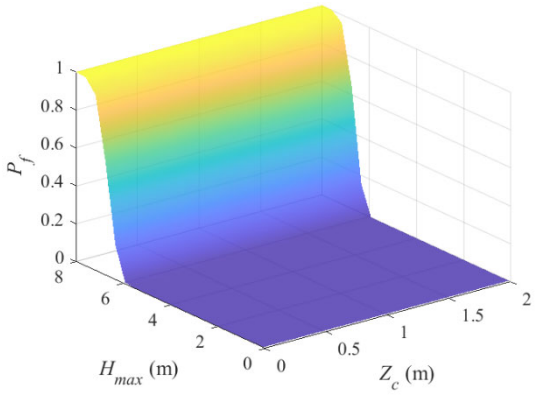

Figure 36. Uplift fragility surface: Suchithra and Koola (1995) (Min)

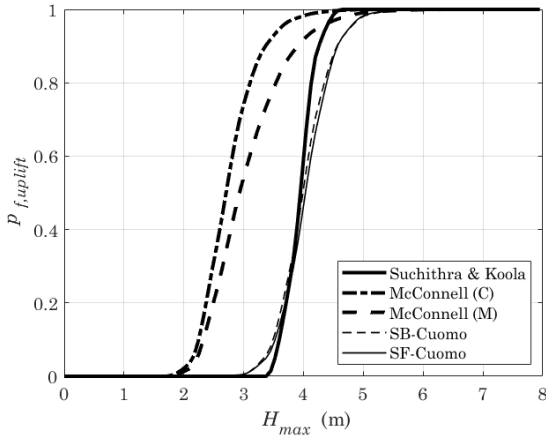

Figure 37. Uplift fragility curves: $Z_C =$ 0m, Suchithra and Koola, McConnell, Cuomo

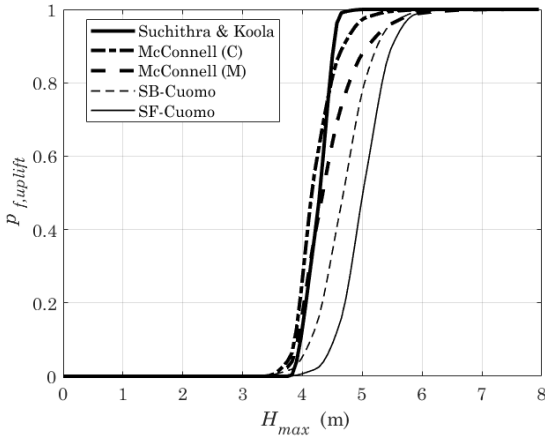

Figure 38. Uplift fragility curves: $Z_C =$ 2m, Suchithra and Koola, McConnell, Cuomo

Table 7 Maximum $p_{f,uplift}$ difference between Suchithra and Koola, McConnell, and Cuomo models

Z_C (m)	Cuomo-Suchithra & Koola (Max)		McConnell-Suchithra & Koola (Max)	
	SB	SF	C	M
0.00	16.38%	20.34%	90.26%	73.46%
0.11	21.61%	27.03%	88.76%	71.02%
0.21	24.76%	30.82%	86.51%	67.69%
0.32	26.73%	34.13%	82.65%	64.71%
0.42	29.95%	40.35%	80.92%	60.54%
0.53	33.98%	46.01%	77.45%	57.35%
0.63	37.30%	51.72%	73.24%	51.94%
0.74	40.68%	56.73%	66.48%	47.90%
0.84	42.96%	60.09%	60.53%	43.11%
0.95	47.94%	66.11%	56.72%	38.34%
1.05	51.45%	71.63%	58.93%	39.24%
1.16	53.37%	72.18%	57.43%	37.85%
1.26	56.46%	75.32%	57.65%	38.34%
1.37	56.64%	76.30%	54.95%	36.46%
1.47	55.03%	72.36%	51.86%	34.35%
1.58	55.62%	72.41%	45.66%	30.33%
1.68	48.64%	72.15%	35.98%	22.96%
1.79	46.49%	76.29%	23.66%	19.89%
1.89	49.72%	80.78%	21.22%	23.65%
2.00	53.13%	83.92%	17.30%	26.10%

Note: SB=SB-Cuomo; SF=SF-Cuomo; C=McConnell (C); M=McConnell (M).

Finally, the uplift fragility surface adopting the Bea et al. (1999) model (Figure 39) is also not significantly affected by changes in surge elevation. For a deck at the water level the maximum difference in the uplift probability between the Bea et al. (1999) model and the Cuomo et al. (2007) model is 99.25% and 99.42% for a seaward deck with beams (SB-Cuomo) and for a seaward flat deck (SF-Cuomo), respectively (Figure 40), while the same differences drop to 95.85% and 91.74% for a deck 2m above water level. The maximum difference in the uplift probability between the Bea et al. (1999) model and the Suchithra and Koola (1995) model adopting the minimum value of the slamming coefficient ($C_S = 2.5$) is 28.21% for a deck at the water level, and increases to 33.23% for a deck 2m above water (Figure 41). The uplift probability estimates using the Bea et al. (1999) model are less compared to the uplift probability estimates using the McConnell et al. (2004) model or the Cuomo et al. (2007) model, but higher compared to the Suchithra and Koola's (1995) model adopting the minimum value of the slamming coefficient ($C_S = 2.5$). This observation probably reflects the fact that the Bea et al. (1999) model was developed by analyzing oil platforms in the Gulf of Mexico and it is used for estimating wave forces on offshore pile-supported deck platforms. Thus, the Bea et al. (1999) model may not be suitable for estimating wave forces on pile-supported decks close to the shore.

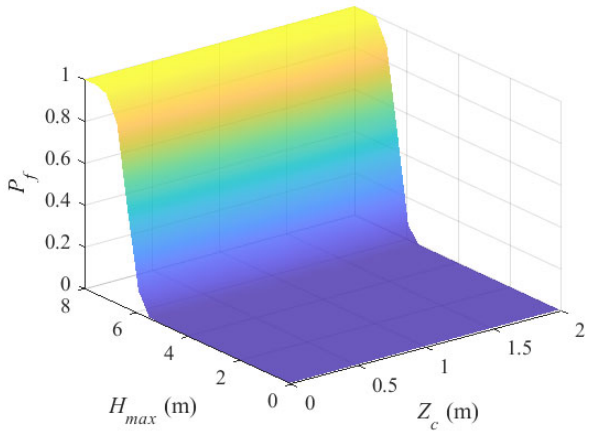

Figure 39. Uplift fragility surface: Bea et al. (1999)

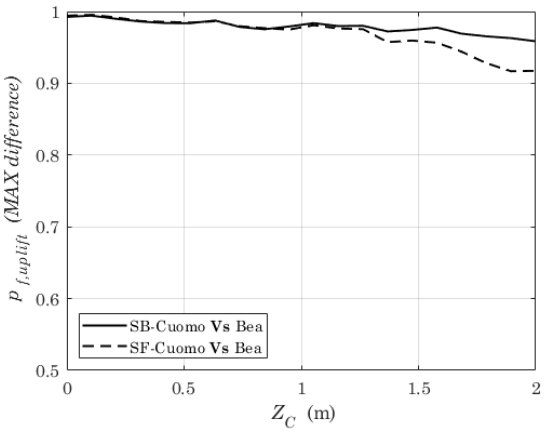

Figure 40. Maximum $p_{f,uplift}$ difference between Cuomo and Bea.

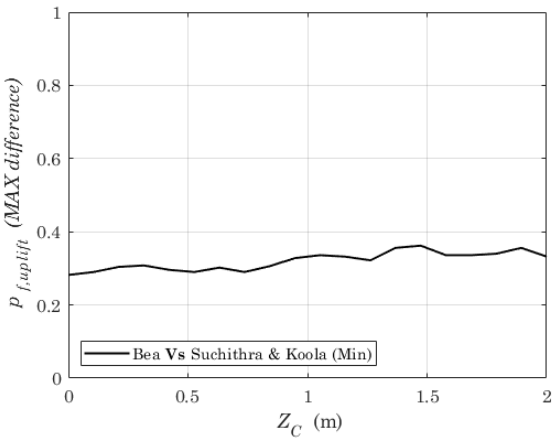

Figure 41. Maximum $p_{f,uplift}$ difference between Bea and Suchithra and Koola (Min).

4.4. Parameterized Fragility Models

As previously mentioned in section 3.2, in parameterized fragility analysis the probability of a limit state function violation is also conditioned upon a set of structural parameters, such as the structure's geometry and material properties. Thus, parameterized fragility analysis can provide risk estimates for a wide range of structures towards the risk assessment across a region (Balomenos et al. 2020). Thus, Maniglio et al. (2021) developed parameterized fragility models for ports subjected to hurricane loads adopting the McConnell et al. (2004) wave model. However, this research observes differences in the probability of uplift between the McConnell et al. (2004) and the Cuomo et al. (2007) wave models, and also a lower sensitivity to storm surge of the wave models that relying on wave kinematics in general. Thus, this research extends those predictions provided by Maniglio et al. (2021), by developing parameterized fragility models for uplift adopting the Cuomo et al. (2007) wave model.

4.4.1. Training of the parameterized fragility models

For the purpose of training the parameterized fragility models, the Monte Carlo simulation (MCS) method is used, similarly to the fragility analysis modeling procedure described in section 4.2.3, for creating a number of samples related to the wave load and structural parameters.

More specifically, a sample of 10,000 values is created for both the maximum wave height H_{max} and relative storm surge Z_C, considering both as uniformly distributed within their sample space. Next, a sample of 10,000 values for the wave period T_p is generated adopting

the same process as described in section 4.2.3, followed by the calculation of the wavelength L_m (Eq. (2) and the maximum crest elevation η_{max} (Eq. (10)). The depth d_s (i.e., the vertical distance between the decks' underside and the seabed) is also considered uniform. Next, 10,000 samples for each of the structural parameters is created, where the deck width b_w, length b_l and thickness b_t are considered uniformly distributed, as well as the pile diameter d_p, the number of dowels n_b and the dowels' diameter d_{se}. Finally, the concrete compressive strength f_c', concrete volume weight γ_C and steel yield strength f_y are sampled following the same process as described in section 4.2.3. Thus, for each simulation, the capacity and demand can be evaluated deterministically, and each simulation can be binary categorized as fail/not fail. Table 8 shows the lower and upper bounds of the structural parameters and the wave parameters adopted for training the parameterized fragility models. Those range of parameters are representative for typical pile-supported wharves and piers for the Houston Ship Channel, in Houston, Texas (Maniglio et al. 2021). Also, a schematic of the process described above is presented in Figure 42.

Table 8 Statistical properties of the predictors

Parameter	Description	Distribution	Lower bound	Upper bound	Mean	COV
Z_C	Relative storm surge	*"Uniform"*	- 5 m	+ 5 m	-	-
H_{max}	Maximum wave height	*"Uniform"*	0.01 m	10.00 m	-	-
d	Pile height	*"Uniform"*	8 m	20 m	-	-
b_w	Deck width	*"Uniform"*	3.00 m	12.70 m	-	-
b_l	Deck length	*"Uniform"*	1.52 m	9.65 m	-	-
b_t	Deck thickness	*"Uniform"*	0.40 m	0.97 m	-	-
d_p	pile diameter	*"Uniform"*	0.81 m	1.32 m	-	-
n_b	Number of dowels	*"Uniform"*	8	16	-	-
d_{se}	Dowels diameter	*"Uniform"*	0.025 m	0.036 m	-	-
f_c'	Concrete compressive strength	*"Normal"*	-	-	55 Mpa	0.09
γ_c	Concrete volume weight	*"Normal"*	-	-	24 kN/m^3	0.04
f_y	Steel yield strength	*"Lognormal"*	-	-		
T_p	wave period corresponding to H_{max}	*"Longuet-Higgings"*	90% T_m	100% T_m	-	-

Note: COV = coefficient of variation.

0

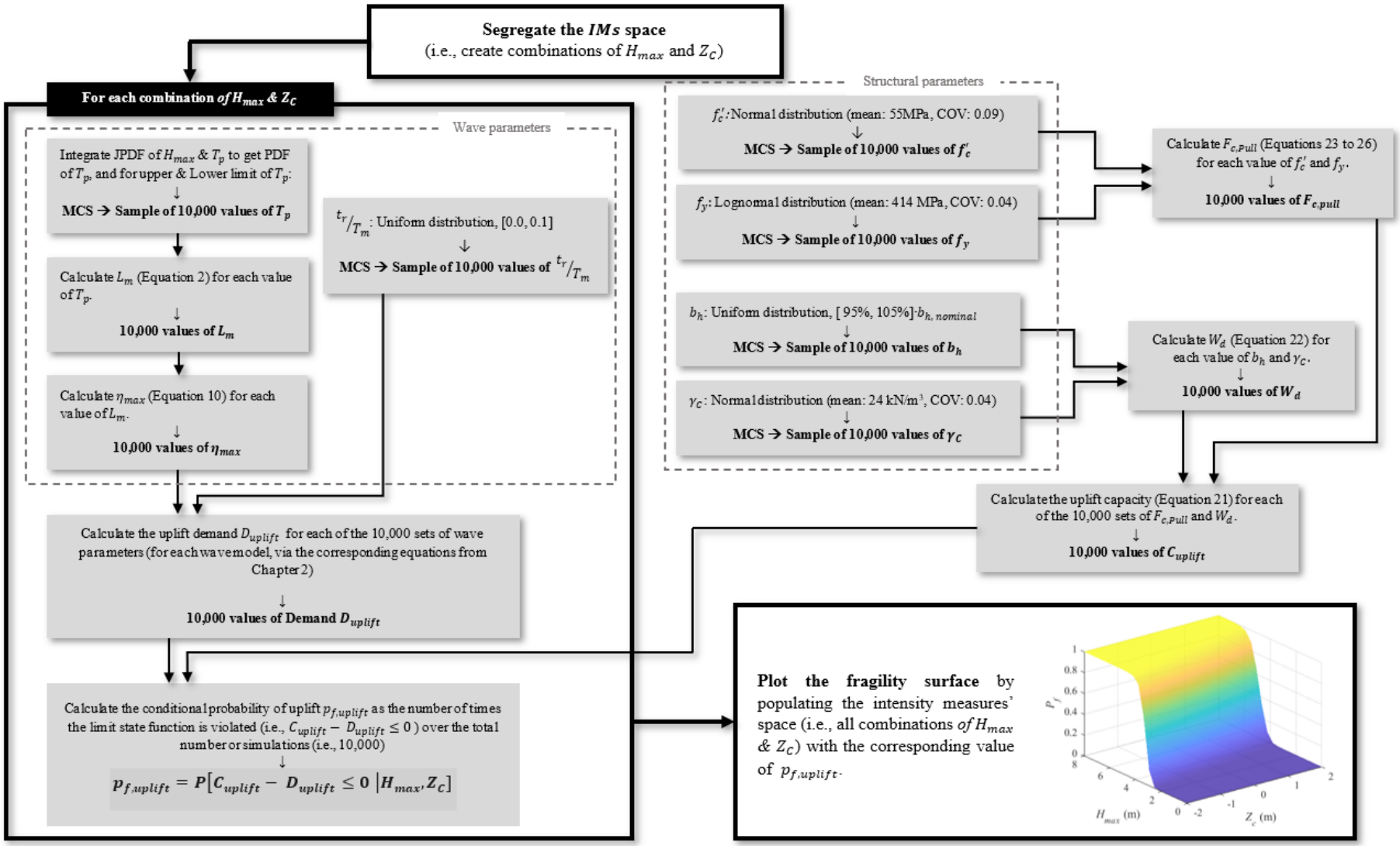

Figure 42 Schematic of the training process for the parameterized fragility models.

1

4.4.2. Goodness-of-fit measures

One of the most common and informative goodness-of-fit measures for classification models is the misclassification error (ME). The misclassification error is defined as the ratio of the objects that were misclassified over the total number of samples. Another simple way to validate a classification model is the accuracy of the model (AC), which is defined as (1-ME). The confusion matrix is also widely used in classification problems. Confusion matrix is comparing the actual class of an object over the predicted class. Thus, the diagonal of the confusion matrix represents the correct predictions, and off-diagonal elements represent misclassification. For the case of binary classification (i.e., fail/not fail) the confusion matrix is a two-by-two matrix, where true positive (TP) and true negative (TN) indicate correct predictions, and false negative (FN) and false positive (FP) indicate wrong predictions. Table 9 shows the confusion matrices for the examined statistical models. Finally, additional goodness-of-fit measures can be derived from the confusion matrix, i.e., the true positive rate (TPR) which is the rate in which the model predicts the positive cases correctly; the true negative rate (TNR) which is the rate in which the model predicts the positive cases correctly; the false positive rate (FPR) which is the rate in which the model erroneously predicts negative cases (not fails) as positives (fails); the false negative rate (FNR) which is the rate in which a model misclassifies a positive case (fail) as negative (not fail). Such measures can be more informative than accuracy (AC) or precision (PR) for models that are biased towards one class, and these metrics are defined as

$$TPR = \frac{TP}{FN + TP};\ TNR = \frac{TN}{TN + FP};\ FPR = \frac{FP}{TN + FP};\ FNR = \frac{FN}{FN + TP} \quad (32)$$

Table 10 and Table 11 summarizes all the goodness-of-fit measures for the examined parameterized fragility models for uplift failure for the case of flat decks (SF-Cuomo) and decks with beams (SB-Cuomo).

Table 9 Confusion matrices for uplift for selected parameterized fragility models

		SLR		SVM (quadratic kernel)		DT (N=100)		KNN (k=100)	
		Predicted class		Predicted class		Predicted class		Predicted class	
	Actual class	Failure	No failure	Failure	No failure	Failure	No failure	Failure	No failure
SF-Cuomo	Failure	3053	235	3047	243	2753	579	2526	708
	No failure	210	6502	201	6509	431	6237	85	6681
SB-Cuomo	Failure	3131	214	3026	270	2863	461	2531	787
	No failure	214	6441	224	6480	512	6164	84	6598

Table 10 Goodness-of-fit for uplift for seaward flat deck (SF-Cuomo)

Parameterized fragility model		AC	ME	TPR	TNR	FPR	FNR	PR
SLR		0.956	0.045	0.929	0.035	0.031	0.072	0.936
SVM	Linear	0.939	0.060	0.908	0.045	0.045	0.093	0.909
	Quadratic	0.956	0.044	0.926	0.036	0.030	0.074	0.938
	Cubic	0.942	0.058	0.924	0.038	0.047	0.076	0.903
DT	N=4	0.896	0.104	0.862	0.070	0.088	0.138	0.831
	N=20	0.902	0.098	0.847	0.074	0.071	0.153	0.852
	N=100	0.899	0.101	0.826	0.085	0.065	0.174	0.865
KNN	k=1	0.834	0.166	0.739	0.128	0.119	0.261	0.755
	k=10	0.892	0.108	0.745	0.118	0.034	0.255	0.917
	k=100	0.9207	0.079	0.781	0.096	0.013	0.219	0.967

Note: AC=Accuracy; ME = Misclassification Error; TPR = True Positive Rate; TNR= True Negative Rate; FPR = False Positive Rate; FNR = False Negative Rate; PR=Precision;.

0

Table 11 Goodness-of-fit for uplift for seaward deck with beams (SB-Cuomo)

Parameterized fragility model		AC	ME	TPR	TNR	FPR	FNR	PR
SLR		0.957	0.043	0.936	0.032	0.032	0.064	0.936
SVM	Linear	0.937	0.063	0.901	0.050	0.045	0.099	0.910
	Quadratic	0.951	0.049	0.918	0.040	0.033	0.082	0.931
	Cubic	0.944	0.056	0.921	0.039	0.045	0.079	0.909
DT	N=4	0.891	0.109	0.849	0.077	0.088	0.151	0.829
	N=20	0.900	0.100	0.848	0.077	0.073	0.152	0.856
	N=100	0.903	0.097	0.861	0.069	0.077	0.139	0.848
KNN	k=1	0.835	0.165	0.758	0.119	0.128	0.242	0.743
	k=10	0.896	0.104	0.756	0.111	0.035	0.245	0.914
	k=100	0.913	0.087	0.763	0.107	0.013	0.237	0.968

Note: AC=Accuracy; ME = Misclassification Error; TPR = True Positive Rate; TNR= True Negative Rate; FPR = False Positive Rate; FNR = False Negative Rate; PR=Precision;.

1

4.4.3. Parameterized fragility models using SLR

The examined parameterized fragility models perform similarly in terms of accuracy in prediction, with SMV with quadratic kernel and SLR having the highest goodness-of-fit metrics. Additionally, SLR provides a closed form solution for estimating the probability of uplift failure, and thus, it is selected for the proposed parameterized fragility models. Equations (33 and (34 show the proposed parameterized fragility models for the case of seaward flat decks (SF-Cuomo) and seaward decks with beams (SB-Cuomo), respectively.

$$
\begin{aligned}
&g(H_{max}, Z_C, d, b_w, b_l, b_t, n_b, d_{se}) \\
&\quad = -5.5573 + 4.1308H_{max} - 1.8787Z_C - 0.0206d + 1.2898b_w \\
&\quad + 1.9920b_l - 3.2329b_t - 1.1199n_b - 764.8800d_{se} \\
&\quad + 0.1213H_{max}Z_C - 0.0746H_{max}d - 0.0720b_wb_l + 0.0408b_wn_b \\
&\quad + 25.0390b_wd_{se} + 0.0551b_ln_b + 34.4790b_ld_{se} - 0.0785Z_C^2 \\
&\quad - 0.0824b_w^2 - 0.1731\, b_l^2
\end{aligned}
\tag{33}
$$

$$
\begin{aligned}
&g(H_{max}, Z_C, d, b_w, b_l, b_t, n_b, d_{se}) \\
&\quad = 1.4596 + 3.4320H_{max} - 1.1679Z_C - 0.3265d + 1.2517b_w \\
&\quad + 2.2803b_l - 11.5110b_t - 0.9625n_b - 771.7400d_{se} \\
&\quad + 0.1051H_{max}Z_C + 0.1261H_{max}b_l + 1.0624H_{max}b_t - 0.0481Z_Cb_l \\
&\quad + 0.0369b_wn_b + 28.3430b_wd_{se} - 0.1443H_{max}^2 - 0.0549Z_C^2 \\
&\quad - 0.0930b_w^2 - 0.1321\, b_l^2
\end{aligned}
\tag{34}
$$

While both models are having very high true positive (TPR) and true negative (TNR) rates (Table 10, Table 11), Equation (33 is more biased towards no failure. For example, in 10,000 simulations, Equation (33) predicts no failure 235 times, although failure occurs, and failure 210 times, although no failure occurs (Table 9). Additionally, as expected, in both models the storm intensity (Z_C, H_{max}) and capacity parameters (n_b, d_{se} and the weight of the deck in terms of b_l, b_w, b_t) affect the failure estimate. However, the depth d_s appears to also affect the uplift estimate, reducing the probability of uplift for higher water depths. Finally, there might be some imbalanced number of observations within the two classes (Table 9) (e.g., for the case of flat decks (SF-Cuomo) 3,053 failures and 6,502 no failures, and for the case of deck with beams (SB-Cuomo) 3,131 failures and 6,441 no failures). However, the number of observations is not significantly imbalanced.

5. Discussion and Conclusions

5.1. Summary

This research aims to shed light on the sensitivity of the uplift fragility of pile-supported port structures for a range of different wave models. The examined failure mode is the uplift of the deck-pile connections subjected to vertical forces induced by storm surge and waves. For each examined wave model, a Monte Carlo simulation is conducted, and the uplift probability is evaluated for different combinations of surge elevation and wave height. Thus, the fragility surface for each wave model is plotted as the uplift probability conditioned on the maximum wave height and surge elevation.

In the second part of this research, several statistical learning techniques are examined with the purpose of developing parameterized fragility models for the examined failure mode. For training the parameterized fragility models, a Monte Carlo simulation is utilized to create a sample-space of wave load and structural parameters. Finally, this research develops parameterized fragility models using stepwise logistic Regression (SLR), to allow rapid cross-regional risk assessment of pile-supported ports.

5.2. Conclusions

Based on the fragility analysis results and the parameterized fragility models, this research found that:

- The results indicate that the uplift probability estimate is highly sensitive to the wave model selection, reflecting the challenge in estimating the complex in nature hydraulic loads.

- Depending on the Wave Model selection, the IMs may differ. Empirical wave models (i.e., Wang (1970), McConnell et al. (2004) , Cuomo et al. (2007)) are more sensitive to the storm surge compared to semi-empirical wave models (i.e., Kaplan et al. (1995), Suchithra and Koola (1995), Bea et al. (1999)). While H_{max} and Z_C are the most important IMs for predicting uplift, for the examined range of IMs, that does not reflect to semi-empirical wave models, thus 2D fragility curves may be constructed for those models (i.e., Z_C may not change/affect the probability of uplift).
- Empirical wave models are more conservative compared to semi-empirical, especially for higher surge elevation (i.e., for smaller clearance).
- Finally, this research provides parameterized fragility models, for the case of flat decks and decks with beams. As expected, similarly to previous work, the parameterized fragility models indicate that the storm intensity measures and the structure's geometry are the most informative parameters for the prediction of the probability of uplift. But furthermore, compared to previous work, the parameterized fragility models also include an additional predictor (i.e., the water depth d) indicating that the wave model adopted may also be sensitive to the water depth. Thus, depending on the Wave Model selection the predictors for the parameterized fragility might change.

5.3. Future Work

Due to the complexity of the underside construction of the pile-supported deck and the potential of existing opening, future work may:

- Develop fluid-structure interaction models, that can further explore the effect of underside roughness in estimating the probability of uplift.
- Further investigate the effect of entrapped air in the estimated probability of uplift.

Furthermore, while the parameterized fragility models provided herein are applicable to a wide range of pier geometries, water depths and dowelled connections (i.e., number and diameter of dowels), they are applicable only for this type of connection (i.e., doweled deck-pile connection). Thus, future work may:

- Develop parameterized fragility models for different types of connections (e.g., extended strand, hollow dowelled, etc.).
- Explore the effect of time dependent effects (i.e., aging) on the capacity estimate for different type of connections, enabling the application of the presented framework not only for new, but also for existing aged structures.

NOTATIONS

The following symbols are used in this thesis:

A	=	surface area of obstruction to normal flow;
AC	=	accuracy (confusion matrix);
A_{Se}	=	dowel cross-section area;
A_w	=	wetted surface area;
b_h	=	horizontal element thickness;
b_l	=	horizontal element length;
b_w	=	horizontal element width;
C	=	wave celerity;
C_D	=	drag coefficient;
C_i	=	structural capacity;
C_M	=	inertia coefficient;
C_{ns}	=	modified slamming coefficient;
C_S	=	slamming coefficient;
C_{uplift}	=	deck–pile uplift capacity;
d	=	static depth;
D_i	=	structural demand;
dl/dt	=	equals to wave celerity C;
d_p	=	pile diameter;
d_s	=	water depth during storm surge;
d_{se}	=	dowel diameter;
D_{uplift}	=	deck–pile uplift demand;
f	=	Longuet-Higgins joint probability distribution;
$F_{boyancy}$	=	buoyancy force;
f_c'	=	concrete compressive strength;
$F_{C,pull}$	=	connection pullout strength;
F_v^*	=	vertical basic wave force;
$F_{v,imp}$	=	vertical impact force;
$F_{v,qs}$	=	vertical quasi-static force;
$F_{v,total}$	=	total vertical uplift force;
f_y	=	steel yield strength;
g	=	gravitational acceleration;
G_i	=	limit-state function;
G_{uplift}	=	limit-state function for uplift;
H	=	wave height;
H_{max}	=	maximum wave height;

H_s = significant wave height;
i = examined failure mode;
IM = intensity measure;
k = wave number;
L = constant in Longuet-Higgins joint distribution;
l = wetted length;
l_d = development length in tension;
l_{emb} = dowel embedment length;
L_m = wavelength;
m_0 = number of dowels;
n_b = number of dowels;
P = probability;
$p_{f,i}$ = probability of failure;
PR = precision (confusion matrix);
$P_{v,impact}$ = vertical impact pressure;
t = time;
T_m = mean wave period;
T_p = wave period corresponding to H_{max};
t_r = rise time of the event;
$\ddot{w}$ = vertical particle acceleration;
$\dot{w}$ = vertical particle velocity;
W_d = deck weight;
x = horizontal spatial coordinate;
X = vector of structural components;
X_i = parameters of the logistic regression model;
z = vertical spatial coordinate;
Z_C = relative surge elevation (clearance);
$a_{v,imp}$ = coefficient for prediction of vertical impact force;
$\alpha_{v,qs}$ = coefficient for prediction of vertical quasi-static force;
$\beta_{v,imp}$ = coefficient for prediction of vertical impact force;
$\beta_{v,qs}$ = coefficient for prediction of vertical quasi-static force;
γ_C = concrete unit weight;
ε = Model error term;
η = dimensionless wave period;
$\tilde{\eta}$ = wave surface elevation;
η_{max} = maximum crest elevation;
θ_i = regression coefficients;
λ = lightweight concrete modification factor (ACI 318-14);
ν = wave spectral density;
ξ = dimensionless wave height;

ρ = seawater density;
φ_b = bond strength;
ψ_e = reinforcement coating factor (ACI 318-14);
ψ_t = tension casting location factor (ACI 318-14);
ω = wave angular frequency.

REFERENCES

AASHTO. (2008). "*Guide specifications for bridges vulnerable to coastal storms,* Washington, DC.

ACI (American Concrete Institute). (2014). "*Building code requirements for structural concrete." ACI 318-14,* Farmington Hills, MI

Alberto Lamberti ,Luca Martinelli,M. Gabriella Gaeta, M. T. &John A. (2011). Experimental spatial correlation of wave loads on front decks. *Journal of Hydraulic Research*, *Volume 49*.

Allsop, W., Alderson, J., & Cuomo, G. (2009). Why do suspended deck coastal structures keep failing? *Forensic Engineering, Proceedings of the Congress*, *January 2016*, 191–203. https://doi.org/10.1680/fefftu.36130.0019

Altman, N. S. (1992). An Introduction to Kernel and Nearest-Neighbor Nonparametric Regression. *The American Statistician*, *46*(3), 175–185. https://doi.org/10.1080/00031305.1992.10475879

API (American Petroleum Institute). (2000). *Recommended practice for planning, designing and constructing fixed offshore platforms–working stress design.* RP 2A-WSD,Washington, DC.

ASCE (2014). "*Seismic design of piers and wharves*." ASCE/COPRI 61-14, Reston, VA.

Ataei, N., & Padgett, J. (2013). Probabilistic Modeling of Bridge Deck Unseating during Hurricane Events. *Journal of Bridge Engineering*, *18*, 275–286. https://doi.org/10.1061/(ASCE)BE.1943-5592.0000371, 275-286.

Balomenos, G. P., Kameshwar, S., & Padgett, J. E. (2020). Parameterized fragility models for multi-bridge classes subjected to hurricane loads. *Engineering Structures*, *208*, 110213. https://doi.org/https://doi.org/10.1016/j.engstruct.2020.110213

Balomenos, G. P., & Padgett, J. E. (2018a). Fragility Analysis of Pile-Supported Wharves and Piers Exposed to Storm Surge and Waves. *Journal of Waterway, Port, Coastal, and Ocean Engineering*, *144*(2), 04017046. https://doi.org/10.1061/(asce)ww.1943-5460.0000436

Balomenos, G., & Padgett, J. (2018b). *Vulnerability Assessment of Port Structures Subjected to Storm Surge and Waves*. ,Proc., ASCE Structures Congress 2018, Fort Worth, TX. https://doi.org/10.1061/9780784481325.036

Balomenos, G. P., & Padgett, J. E. (2018c). Effects of Wave Loading Conditions on the Fragility of Pile-Supported Wharves/Piers. *Coastal Engineering Proceedings*, *36*, 29. https://doi.org/10.9753/icce.v36.structures.29

Bardi, J. C., Ostbo, B. I., Fenical, S., & Tirindelli, M. (2007). Cozumel's International Cruise Terminal: Hurricane Wilma Recovery and Reconstruction. *Ports 2007*, 1–10. https://doi.org/10.1061/40834(238)71

Bea, R G, Iversen, R., & Xu, T. (2000). Wave-in-Deck Forces on Offshore Platforms . *Journal of Offshore Mechanics and Arctic Engineering*, *123*(1), 10–21. https://doi.org/10.1115/1.1342160

Bea, Robert G, Xu, T., Stear, J., & Ramos, R. (1999). Wave Forces on Decks of Offshore Platforms. *Journal of Waterway Port Coastal and Ocean Engineering-Asce*, *125*, 136–144.

Bender, C., Smith, J., Kennedy, A., & Jensen, R. (2013). STWAVE simulation of Hurricane Ike: Model results and comparison to data. *Coastal Engineering*, *73*, 58–70. https://doi.org/10.1016/j.coastaleng.2012.10.003

Breiman, L., Friedman, J. H., Olshen, R. A., & Stone, C. J. (2017). *Classification and regression trees*. Routledge.

BROUGHTON, P., & HORN, E. (1987). EKOFISK PLATFORM 2/4C: RE-ANALYSIS DUE TO SUBSIDENCE. *Proceedings of the Institution of Civil Engineers*, *82*(5), 949–979. https://doi.org/10.1680/iicep.1987.488

Cornett, A. (2013). Wave-in-Deck Loads for an Intricate Pile-Supported Pier and Variation With Deck Clearance. In *Proceedings of the International Conference on Offshore Mechanics and Arctic Engineering - OMAE* (Vol. 1). https://doi.org/10.1115/OMAE2013-11409

Cortes, C., & Vapnik, V. (1995). Support-vector networks. *Machine Learning*, *20*(3), 273–297. https://doi.org/10.1007/BF00994018

Cozumel Cruise Port. (n.d.). Https://Www.Viator.Com/. https://www.viator.com/Cozumel-attractions/Cozumel-Cruise-Port/overview/d632-a3282

Cuomo, G., Shimosako, K., & Takahashi, S. (2009). Wave-in-deck loads on coastal bridges and the role of air. *Coastal Engineering*, *56*(8), 793–809. https://doi.org/https://doi.org/10.1016/j.coastaleng.2009.01.005

Cuomo, G., Tirindelli, M., & Allsop, W. (2007). Wave-in-deck loads on exposed jetties. *Coastal Engineering*, *54*(9), 657–679. https://doi.org/10.1016/j.coastaleng.2007.01.010

Dietrich, J. C., Zijlema, M., Westerink, J. J., Holthuijsen, L. H., Dawson, C., Luettich, R. A., Jensen, R. E., Smith, J. M., Stelling, G. S., & Stone, G. W. (2011). Modeling hurricane waves and storm surge using integrally-coupled, scalable computations. *Coastal Engineering*, *58*(1), 45–65. https://doi.org/https://doi.org/10.1016/j.coastaleng.2010.08.001

Douglass SL, Chen Q, Olsen JM, Edge BL, B. D. (2006). *Wave forces on bridge decks. Final report prepared for US Department of Transportation and Federal Highway Administration Office of Bridge Technology*.

El Ghamry, O. A. (1963). *Wave forces on a dock* (B. University of California & U. States (Eds.)). Berkeley: University of California, Hydraulic Engineering Laboratory, Wave Research Projects.

Forschungs-Zentrum Küste (FZK). (n.d.). https://www.fzk.uni-hannover.de/

Freeman, S. (2020, July 28). *Bob Hall Pier Closed Until Further Notice*. https://www.ccbiznews.com/

French, J. A. (1969). *Wave uplift pressures on horizontal platforms*. Technical Report R546. U.S. Naval Civil Engineering Laboratory, June, 1967.

Gaeta, M., Martinelli, L., & Lamberti, A. (2012). Uplift forces on wave exposed jetties: Scale comparison and effect of venting. *Coastal Engineering Proceedings*, *1*. https://doi.org/10.9753/icce.v33.structures.34

Gutierrez, C. M., Cresanti, R., & Jeffrey, W. A. (2006). Performance of Physical Structures in Hurricane Katrina and Hurricane Rita: A Reconnaissance Report. *NIST Technical Note 1476, National Institute of Standards and Technology, Washington, DC.*

Harn, R., Mays, T. W., and Johnson, G. S. (2010). Proposed seismic detailing criteria for piers and wharves. *ASCE Ports 2010: Building on the Past, Respecting the Future, ASCE, Reston, VA, 460-469.*

Hosmer Jr, D. W., Lemeshow, S., & Sturdivant, R. X. (2013). *Applied logistic regression* (Vol. 398). John Wiley & Sons, New York.

JCSS (Joint Committee on Structural Safety). (2001). *JCSS probabilistic model code.*

Kaplan, P., Murray, J. J., & Yu, W. (1995). Theoretical analysis of wave impact forces on platform deck structures. *OMAE 1995 : Proceedings of the 14th International Conference on Offshore Mechanics and Arctic Engineering ;*, 189–198.

Kaplan, Paul. (1992). *Wave Impact Forces on Offshore Structures: Re-Examination and New Interpretations*. https://doi.org/10.4043/6814-MS

Longuet-Higgins, M. S. (1983). On the joint distribution of wave periods and amplitudes in a random wave field. *Proceedings of the Royal Society of London. A. Mathematical and Physical Sciences*, *389*, 241–258.

MacGregor, J. G., & Wight, J. K. (2005). *Reinforced concrete: Mechanics and design*. Pearson Prentice Hall, Upper Saddle River, NJ.

Maniglio, M., Balomenos, G. P., Padgett, J. E., & Cimellaro, G. P. (2021). Parameterized coastal fragilities and their application to aging port structures subjected to surge and wave. *Engineering Structures*, *237*(March), 112235. https://doi.org/10.1016/j.engstruct.2021.112235

Martin Associates. (2019). *2018 National Economic Impact of the U.S. Coastal Port System: Executive Summary*.

Massel, S. R. (1996). *Ocean surface waves: Their physics and prediction*. World Scientific, River Edge, NJ.

McConnell, K., Allsop, W., and Cruickshank, I. (2004). *Piers, jetties and related structures exposed to waves: guidelines for hydraulic loadings* (Thomas Telford (Ed.)).

McConnell, K.J., Allsop, N.W.H., Cuomo, G., Cruickshank, I. C. (2003). New guidance for wave forces on jetties in exposed locations. *COPEDEC VI, Colombo, Sri Lanka*, 20 pp.

McConnell, K., Allsop, N., Cuomo, G., & Cruickshank, I. (2003). New Guidance for Wave Forces on Jetties in Exposed Locations. *Copedec Vi*, *040*, 1–20.

McKay, M. D., Beckman, R. J., & Conover, W. J. (1979). A Comparison of Three Methods for Selecting Values of Input Variables in the Analysis of Output from a Computer Code. *Technometrics*, *21*(2), 239–245. https://doi.org/10.2307/1268522

McKenna, F., Fenves, G. L., & Scott, M. H. (2000). *Open system for earthquake engineering simulation.* University of California, Berkeley.

Metropolis, N., & Ulam, S. (1949). The Monte Carlo Method. *Journal of the American Statistical Association*, *44*(247), 335–341. https://doi.org/10.2307/2280232

Morison, J. R., Johnson, J. W., & Schaaf, S. A. (1950). The Force Exerted by Surface Waves on Piles. *Journal of Petroleum Technology*, *2*(05), 149–154. https://doi.org/10.2118/950149-G

Nowak, A. S., and Collins, K. R. (2000). Reliability of structures, McGraw- Hill, New York.

Nowak, A., Rakoczy, A., & Szeliga, E. K. (2011). Revised statistical resistance models for R/C structural components. *American Concrete Institute, ACI Special Publication*, *284*, 61–76.

Nowak, A. S., and Szerszen, M. M. (2003). "Calibration of design code for buildings (ACI 318): Part 1—Statistical models for resistance." *ACI Struct. J., 100(3), 377–382.*

POLB (Port of Long Beach). (2012). *Wharf design criteria, version 3.0,* Long Beach, CA.

Port of Dampier. (n.d.). Pilbara Ports Authority, Australia. https://www.pilbaraports.com.au/ports/port-of-dampier

Porter, K. (2021). *A Beginner's Guide to Fragility, Vulnerability, and Risk* (p. 139). University of Colorado Boulder. https://www.sparisk.com/pubs/Porter-beginners-guide.pdf

Seiffert, B., Hayatdavoodi, M., & Ertekin, R. C. (2014). Experiments and computations of solitary-wave forces on a coastal-bridge deck. Part I: Flat Plate. *Coastal Engineering*, *88*, 194–209. https://doi.org/10.1016/j.coastaleng.2014.01.005

Shih, & Anastasiou, K. (1992). A laboratory study of the wave-induced vertical loading on platform decks. *Proceedings of the Institution of Civil Engineers - Water, Maritime and Energy*, *96*(1), 19–33. https://doi.org/10.1680/iwtme.1992.09778

Sorensen, R. M. (1993). *Basic Coastal Engineering: For coastal and ocean engineers*. John Wiley& Sons, New York.

Stringer, S., & Harn, R. (2012). Seismic stability of marine piers built with prestressed concrete piles. *American Concrete Institute, ACI Special Publication*, *295*(295 SP), 62–82. https://doi.org/10.14359/51686346

Sturgis, L. a., Smythe, T., & Tucci, A. (2014). Port Recovery in the Aftermath of Hurricane Sandy: Improving Port Resiliency in the Era of Climate Change. *Center for a New American Security*, *August 2014*, 5–21.

Suchithra, N., & Koola, P. M. (1995). A study of wave impact of horizontal slabs. *Ocean Engineering*, *22*(7), 687–697. https://doi.org/https://doi.org/10.1016/0029-8018(95)00001-2

Szerszen, A. S. N. and M. M. (n.d.). Calibration of Design Code for Buildings (ACI 318): Part 1—Statistical Models for Resistance. *ACI Structural Journal*, *100*(3). https://doi.org/10.14359/12613

Tirindelli, M., Cuomo, G., Allsop, N.W.H., McConnell, K.J. (2003). Physical model studies of wave-induced forces on exposed jetties: towards new prediction formulae. *Proc. Conf. Coastal Structures 2003. ASCE/COPRI, Portland*, 382–393.

Tirindelli, M., Cuomo, G., Allsop, W., & Lamberti, A. (2003). Wave-in-Deck Forces on Jetties and Related Structures. *Proceedings of the International Offshore and Polar Engineering Conference*, *January*, 2812–2819.

Tirindelli, M., Cuomo, G., Allsop, W., & McConnell, K. (2003). *Exposed Jetties: Inconsistencies and Gaps in Design Methods for Wave-Induced Forces*. *March 2003*, 1684–1696. https://doi.org/10.1142/9789812791306_0142

Toumazis, A. D., Shih, R., & Anastasiou, K. A. (1989). Wave impact loading on horizontal and vertical plates. *Proc. of IAHR 89 Conf., Ottawa, Canada*, c209–c216.

UNCTAD. (2019). *Review of Maritime Transport 2019*. https://unctad.org/

UNCTAD. (2020). *Review of Maritime Transport 2020*. https://unctad.org/

Wang, Hsian. (1967). *ESTIMATING WAVE PRESSURES ON A HORIZONTAL PIER*. Technical Report R546. U.S. Naval Civil Engineering Laboratory, June, 1967.

Wang, Hsiang. (1970). Water Wave Pressure on Horizontal Plate. *Journal of Hydraulic Engineering*, *96*, 1997–2017.

https://thisiscozumel.com (2014). *Work Starts On New Cozumel Pier*, https://thisiscozumel.com/news/70-latest-news/1553-new-cozumel-cruise-pier